*Astronomy & Astrophysics* manuscript no. cosmology2_report
April 24, 2023 

# Calculate the CMB power spectrum: Cosmology II

Johan Mylius Kroken[1, 2]

[1] Institute of Theoretical Astrophysics (ITA), University of Oslo, Norway
[2] Center for Computing in Science Education (CCSE), University of Oslo, Norway

April 24, 2023 GitHub repo link: https://github.com/Johanmkr/AST5220/tree/main/project

**ABSTRACT**

SOME ABSTRACT

## Contents

**1 Introduction** **2**

**2 Milestone I - Background Cosmology** **2**
2.1 Theory . . . 2
2.1.1 Fundamentals . . . 2
2.1.2 Measure of time and space . . . 3
2.1.3 ΛCDM-model . . . 4
2.1.4 Analytical solutions and sanity checks . . . 4
2.2 Methods . . . 5
2.2.1 ODEs and Splines . . . 5
2.2.2 Fit to supernova data . . . 5
2.3 Results and discussion . . . 5
2.3.1 Tests . . . 5
2.3.2 Analysis . . . 6

**3 Milestone II - Recombination History** **8**
3.1 Theory . . . 8
3.1.1 Hydrogen recombination . . . 9
3.1.2 Visibility . . . 10
3.1.3 Sound horizon . . . 10
3.2 Methods . . . 10
3.2.1 Computing $X_e$ . . . 10
3.2.2 Computing $\tau$ and $\tilde{g}$ . . . 10
3.2.3 Analysis . . . 11
3.3 Results and discussion . . . 11
3.3.1 Times and sound horizon . . . 11
3.3.2 Free electron fraction . . . 11
3.3.3 Visibility . . . 11
3.3.4 General discussion . . . 12

**4 Milestone III - Perturbations** **12**
4.1 Theory . . . 12
4.1.1 Metric perturbations . . . 12
4.1.2 Fourier space and multipole expansion . . . 13
4.1.3 Einstein-Boltzmann equations . . . 13
4.1.4 Tight coupling regime . . . 14
4.1.5 Inflation . . . 15
4.1.6 Initial conditions . . . 16
4.2 Methods . . . 16
4.3 Results and discussion . . . 16

**A Useful derivations** **17**
A.1 Angular diameter distance . . . 17
A.2 Luminosity distance . . . 17
A.3 Differential equations . . . 17

**B Sanity checks** **17**
B.1 For $\mathcal{H}$ . . . 17
B.2 For $\eta$ . . . 17

## Nomenclature

### Constants of nature

$m_e$ - Mass of electron.
$m_e = 9.10938356 \cdot 10^{-31}$ kg.
$m_{\rm H}$ - Mass of hydrogen atom.
$m_{\rm H} = 1.6735575 \cdot 10^{-27}$ kg.
$G$ - Gravitational constant.
$G = 6.67430{\cdot}10^{-11}$ m$^3$ kg$^{-1}$ s$^{-2}$.
$k_B$ - Boltzmann constant.
$k_B = 1.38064852 \cdot 10^{-23}$ m$^2$ kg s$^{-2}$ K$^{-1}$.
$\hbar$ - Reduced Planck constant.
$\hbar = 1.054571817 \cdot 10^{-34}$ J s$^{-1}$.
$c$ - Speed of light in vacuum.
$c = 2.99792458 \cdot 10^8$ m s$^{-1}$.
$\sigma_T$ - Thomson cross section.
$\sigma_T = 6.6524587158 \cdot 10^{-29}$ m$^2$.
$\alpha$ - Fine structure constant.
$\alpha = \frac{m_e c}{\hbar}\sqrt{\frac{3\sigma_T}{8\pi}}$

### Cosmological parameters

$G_{\mu\nu}$ - Einstein tensor.
$T_{\mu\nu}$ - Stress-energy tensor.
$H$ - Hubble parameter.
$\mathcal{H}$ - Conformal Hubble parameter.
$T_{\rm CMB0}$ - Temperature of CMB today.
$a$ - Scale factor.
$x$ - Logarithm of scale factor.
$t$ - Cosmic time.
$z$ - Redshift.
$\eta$ - Conformal time.
$\chi$ - Co-moving distance.
p - Pressure.
$\rho$ - Density.
$r$ - Radial distance.
$d_A$ - Angular diameter distance.
$d_L$ - Luminosity distance.

---

$n_e$ - Electron density.
$n_b$ - Baryon density.
$X_e$ - Free electron fraction.
$\tau$ - Optical depth.
$\tilde{g}$ - Visibility function.
$s$ - Sound horizon.
$r_s$ - Sound horizon at decoupling.
$c_s$ - Wave propagation speed.

### Density parameters

Density parameter $\Omega_X = \rho_X/\rho_c$ where $\rho_X$ is the density and $\rho_c = 8\pi G/3H^2$ the critical density. $X$ can take the following values:

$b$ - Baryons.
CDM - Cold dark matter.
$\gamma$ - Electromagnetic radiation.
$\nu$ - Neutrinos.
$k$ - Spatial curvature.
$\Lambda$ - Cosmological constant.

A 0 in the subscript indicates the present day value.

### Fiducial cosmology

The fiducial cosmology used throughout this project is based on the observational data obtained by Aghanim et al. (2020):

$$\begin{aligned}
h &= 0.67,\\
T_{\rm CMB0} &= 2.7255 \text{ K},\\
N_{\rm eff} &= 3.046,\\
\Omega_{\rm b0} &= 0.05,\\
\Omega_{\rm CDM0} &= 0.267,\\
\Omega_{k0} &= 0,\\
\Omega_{\nu 0} &= N_{\rm eff}\cdot\frac{7}{8}\left(\frac{4}{11}\right)^{4/3}\Omega_{\gamma 0},\\
\Omega_{\Lambda 0} &= 1-(\Omega_{k0}+\Omega_{\rm b0}+\Omega_{\rm CDM0}+\Omega_{\gamma 0}+\Omega_{\nu 0}),\\
\Omega_{\rm M0} &= \Omega_{b0}+\Omega_{\rm CDM0},\\
\Omega_{\rm rad} &= \Omega_{\gamma 0}+\Omega_{\nu 0},\\
n_s &= 0.965,\\
A_s &= 2.1\cdot 10^{-9}.
\end{aligned}$$

## 1. Introduction

Introduce all for Milestones and the overall aim of calculating the CMB power spectrum etc.

TODO: Obviously this introduction will change and amended as more milestones are completed.

## 2. Milestone I - Background Cosmology

According to the cosmological principle, the universe is homogeneous and isotropic on a large scale. Hence, here are no preferred locations nor directions. Furthermore, we may safely assume that the physical laws that govern our local part of the universe is equally valid elsewhere, at larger distances.

The aim now is to set up the background cosmology, in which the investigation of all interesting phenomena will take place. Setting up the background cosmology is practically equivalent to solving the *Einstein field equation*:

$$G_{\mu\nu} = 8\pi G T_{\mu\nu}, \tag{1}$$

where $G_{\mu\nu}$ is the Einstein tensor describing the geometry of spacetime, $G$ is the gravitational constant and $T_{\mu\nu}$ is the energy and momentum tensor. This equation thus relates the geometry and shape of spacetime itself, to its energy content (matter included). There are many solutions to Eq. (1), but we want the solution to govern a Universe that is spatially isotropic and homogeneous, but may evolve in time. The spacetime metric that satisfies this conditions is the *Friedmann-Lemaître-Robertson-Walker metric* (FLRW)d (Carroll 2019, ch. 8).

We will use this metric in order to describe the background universe, how it may evolve in time, and its history. Also write about the following:

### 2.1. Theory

#### 2.1.1. Fundamentals

If we assume the universe to be homogeneous and isotropic, the line elements d$s$ is given by the FLWR-metric, here in polar coordinates (Weinberg 2008, eq. 1.1.11):

$$ds^2 = -dt^2 + e^{2x}\left[\frac{dr^2}{1-kr^2} + r^2 d\theta^2 + r^2\sin^2\theta d\phi^2\right], \tag{2}$$

where we have introduced $x = \ln(a)$ which will be our primary measure of time.

We further model all forms of energy in the universe as perfect fluids, only characterised by their rest frame density $\rho$ and isotropic pressure $p$, and an equation of state relating the two:

$$\omega = \frac{\rho}{p}. \tag{3}$$

By conservation of energy and momentum we must satisfy $\nabla_\mu T^{\mu\nu} = 0$, which results in the following differential equations for the density of each fluid $\rho_i$, from Winther et al. (2023):

$$\frac{\mathrm{d}\rho_i}{\mathrm{d}t} + 3H\rho_i(1+\omega_i) = 0, \tag{4}$$

where we have introduced the Hubble parameter $H \equiv \dot{a}/a = \mathrm{d}x/\mathrm{d}t$. The solution to Eq. (4) is of the form:

$$\rho_i \propto e^{-3(1+\omega_i)x}, \tag{5}$$

where $\omega_\mathrm{M} = 0$ (matter), $\omega_\mathrm{rad} = 1/3$ (radiation), $\omega_\Lambda = -1$ (cosmological constant) and $\omega_k = -1/3$ (curvature).

With these assumptions, the solution to the Einstein equations, Eq. (1) are the Friedmann equations (Carroll 2019, ch. 8.3), the first of which describes the expansion rate of the universe:

$$H^2 = \frac{8\pi G}{3}\sum_i \rho_i - kc^2 e^{-2x} \tag{6}$$

and the second describe how this expansion rate changes over time:

$$\frac{\mathrm{d}H}{\mathrm{d}t} + H^2 = -\frac{4\pi G}{3}\sum_i\left(\rho + \frac{3p}{c^2}\right). \tag{7}$$

As of now, we are primarily interested in the first Friedmann equation. By introducing the critical density, $\rho_c \equiv 2H^2/(8\pi G)$, we define the density parameters $\Omega_i = \rho_i/\rho_c$. We further define the density $\rho_k \equiv -3kc^2e^{-2x}/(8\pi G)$,[1] which enables us to write Eq. (6) as simply:

$$1 = \sum_i \Omega_i, \tag{8}$$

‘ where the density $\Omega_k$ is included in the sum. From Eq. (5) we know the evolution of the densities in time, and if we assume the density values today, $\Omega_{i0}$, are known (or are free parameters), then Eq. (6) may also be written as:

$$H = H_0\sqrt{\sum_i \Omega_{i0}e^{-3(1+\omega_i)x}}, \tag{9}$$

which is the Hubble equation we will use further.

[1] This is the “density of curvature”, but is in fact not a real density. It is called this because its mathematical behaviour is similar to that of the other (real) densities.

### 2.1.2. Measure of time and space

There are many ways of measuring time in cosmology, and they are often related to spatial quantities. The most common is perhaps the *scale factor* $a$, which describes how the physical size of the universe changes with time. An increasing scale factor signifies an expanding universe and vice versa. Another, computationally more useful way of describing $a$ is through its logarithm $x = \ln a \iff a = e^x$, which is the convention we will stick to eventually.

Another way of measuring the expansion of the Universe is through the *redshift* $z$, which is defined as the change in wavelength of electromagnetic radiation between emitter and observer. Radiation propagates through the Universe, so any expansion (or contraction) would expand (or contract) the wavelength, and this is encapsulated in the redshift $z = \Delta\lambda/\lambda$. It is connected to the scale factor as $1 + z = 1/a$.

Another, perhaps more familiar, time measure is the *cosmic time* $t$. This is the time[2] measured by a stationary observer (relative to the expanding universe). The statement: *The Universe is somewhat 13 billion years old*, is given in cosmic time, i.e. the time we experience on Earth.

Lastly, there is the *conformal time* $\eta$, defined as $\mathrm{d}\eta = c\mathrm{d}te^{-x}$.[3] This is a measure of distance (or rather the time it would take a light ray to traverse said distance) between points in space, where the expansion of space in between the points is taken into account. We use it to define the *particle horizon*, which is the horizon generated by the maximal conformal time elapsed since the Big Bang. This is how “far away” from the Big Bang any light ray could have propagated (expansion of the Universe included). This horizon expands with time, as we would expect, and this is what we mean by conformal time from now on; the extent of the particle horizon, beyond which there cannot be any causal connection to the Big Bang. Thus, this is effectively the size of the causally connected universe.

Let’s express this mathematically, starting with the cosmic time:

$$t = \int_0^a \frac{\mathrm{d}a}{aH} = \int_{-\infty}^x \frac{\mathrm{d}x}{H}. \tag{10}$$

Using the definition of conformal time, we have:

$$\eta = \int_0^a \frac{c\mathrm{d}a}{a^2H} = \int_{-\infty}^x \frac{c\mathrm{d}x}{e^xH} \equiv \int_{-\infty}^x \frac{c\mathrm{d}x}{\mathcal{H}}, \tag{11}$$

where $\mathcal{H} = e^xH$ is defined as the *conformal Hubble parameter*. We may then define the *comoving distance*, $\chi$, as the distance to a point, where we take the expansion of space into account, such that it becomes constant (given no relative motion). In contrast, the proper distance between two points increase as the universe increase, the comoving distance remain constant. It is related to the conformal time, and given by:

$$\chi = \int_1^a \frac{c\mathrm{d}a}{a^2H} = \int_0^x \frac{c\mathrm{d}x}{\mathcal{H}} = \eta_0 - \eta, \tag{12}$$

where $\eta_0$ is the conformal time today, and $\eta$ is the conformal time of the time we are measuring distance to. The radial coordinate in the FLRW line element, Eq. (2), is given in terms of

[2] In seconds, months, years, or any other preferred temporal unit (like the duration of a footbal match ± added time).

[3] The $c$ is sometimes omitted. $\mathrm{d}\eta = \mathrm{d}te^{-x}$ has units of s, but multiplied with $c$ yields the distance traversed by a light ray in this time; which is the particle horizon.

the comoving distance and the curvature today $\Omega_{k0}$ as:

$$r = \begin{cases} \chi \cdot \frac{\sin(\sqrt{|\Omega_{k0}|}H_0\chi/c)}{\sqrt{|\Omega_{k0}|}H_0\chi/c} & \Omega_{k0} < 0 \\ \chi & \Omega_{k0} = 0 \\ \chi \cdot \frac{\sinh(\sqrt{|\Omega_{k0}|}H_0\chi/c)}{\sqrt{|\Omega_{k0}|}H_0\chi/c} & \Omega_{k0} > 0 \end{cases} \tag{13}$$

It is then straigtforward to define the angular diameter distance:

$$d_A = e^x r, \tag{14}$$

and the luminosity distance:

$$d_L = e^{-x} r, \tag{15}$$

both of which are derived in Appendix A. The temporal quantities $\eta$ and $t$ have the following evolutions with $x$:

$$\frac{\mathrm{d}\eta}{\mathrm{d}x} = \frac{c}{\mathcal{H}}. \tag{16}$$

$$\frac{\mathrm{d}t}{\mathrm{d}x} = \frac{1}{H}. \tag{17}$$

Both differential equations are easy to solve numerically. Their derivation may also be found in Appendix A

#### 2.1.3. ΛCDM-model

In the ΛCDM model, the universe consists of matter in terms of baryonic matter ($b$) and cold dark matter (CDM), radiation in terms of photons ($\gamma$) and neutrinos ($\nu$) and dark energy in terms of a cosmological constant (Λ). In addition, we must allow for some curvature ($k$). As a result, the parameters of the model will be the present values of the Hubble rate, $H_0$, the baryon density $\Omega_{b0}$, the cold dark matter density $\Omega_{\mathrm{CDM}0}$, photon density $\Omega_{\gamma 0}$, neutrino density $\Omega_{\nu 0}$, dark energy density $\Omega_{\Lambda 0}$, and the curvature density $\Omega_{k0}$. The present temperature of the cosmic microwave background radiation $T_{\mathrm{CMB}0}$ fixes the radiation density today through:

$$\begin{aligned} \Omega_{\gamma 0} &= \frac{16\pi^3 G}{90} \cdot \frac{(k_b T_{\mathrm{CMB}0})^4}{\hbar^3 c^5 H_0^2}, \\ \Omega_{\nu 0} &= N_{\mathrm{eff}} \cdot \frac{7}{8} \cdot \left(\frac{4}{3}\right)^{4/3} \cdot \Omega_{\gamma 0}. \end{aligned} \tag{18}$$

The total radiation density is $\Omega_{\mathrm{rad}} = \Omega_\gamma + \Omega_\nu$ and the total matter density is $\Omega_{\mathrm{M}} = \Omega_b + \Omega_{\mathrm{CDM}}$.

The Hubble equation from Eq. (9) may be redefined in terms of the conformal Hubble parameter $\mathcal{H}$ as:

$$\begin{aligned} \mathcal{H} &= H_0\sqrt{U} \\ U &\equiv \sum_i \Omega_{i0} e^{-\alpha_i x}, \end{aligned} \tag{19}$$

where we have defined $\alpha_i \equiv (1 + 3\omega_i)$ and $i \in \{\mathrm{M}, \mathrm{rad}, \Lambda, k\}$. Since we know the values of the various $\omega_i$ it follows that:

$$\begin{aligned} \alpha_{\mathrm{M}} &= 1 \\ \alpha_{\mathrm{rad}} &= 2 \\ \alpha_k &= 0 \\ \alpha_\Lambda &= -2 \end{aligned} \tag{20}$$

Given the evolution of the density parameters with time, where the proportionality constant is the present day density, we introduce the *radiation-matter equality*, i.e. the time radiation and matter densities were equal: $\rho_{\mathrm{rad}} = \rho_{\mathrm{M}}$. According to Eq. (5) this can be expressed as:

$$\begin{aligned} &\rho_{\mathrm{rad}0} e^{-4x} = \rho_{\mathrm{M}0} e^{-3x} \\ &\quad e^x = \frac{\rho_{\mathrm{rad}0}}{\rho_{\mathrm{M}0}} \implies x_{\mathrm{rM}} = \ln\left(\frac{\Omega_{\mathrm{rad}0}}{\Omega_{\mathrm{M}0}}\right), \end{aligned} \tag{21}$$

where $x_{\mathrm{rM}}$ now denotes the time of radiation-matter equality.

Similarly, the *matter-dark energy equality*, where $\rho_{\mathrm{M}} = \rho_\Lambda$ can be found to be:

$$\begin{aligned} &\rho_\Lambda = \rho_{\mathrm{M}0} e^{-3x} \\ &\implies x_{\mathrm{M}\Lambda} = \frac{1}{3}\ln\left(\frac{\Omega_{\mathrm{M}0}}{\Omega_\Lambda}\right) \end{aligned} \tag{22}$$

Since $\mathcal{H}$ describes the expansion of the Universe, it is fair to say that the acceleration of the Universe is governed by its second derivative, and the acceleration onset may be found from the extremal point in its first derivative. This means that we find the acceleration onset when:

$$\frac{\mathrm{d}\mathcal{H}}{\mathrm{d}x} = 0 \iff \frac{\mathrm{d}U}{\mathrm{d}x} = 0. \tag{23}$$

This follows from Eq. (19). For further details on the derivative, see Appendix B. We assume dark energy is involved in the acceleration of the universe, and thus assume the contribution from radiation is negligible. Eq. (23) is thus further reduced to:

$$\begin{aligned} &2\Omega_{\Lambda 0} e^{2x} - \Omega_{\mathrm{M}0} e^{-x} = 0 \\ &\quad \implies x_{\mathrm{accel}} = \frac{1}{3}\ln\left(\frac{\Omega_{\mathrm{M}0}}{2\Omega_{\Lambda 0}}\right). \end{aligned} \tag{24}$$

The age of the universe today, and the conformal time today can both be found by evaluating the solutions to the differential equations of $t$ and $\eta$ at the present time (where $x = 0$). This is done numerically.

#### 2.1.4. Analytical solutions and sanity checks

There are several ways we may check that both our workings and numerical implementations are indeed correct. The simplest way is to always ensure that the sum of all density parameters add up to 1, for all times: $\sum_i \Omega_i = 1$.

If we only consider the most dominant density parameter, that is $\Omega_i \gg \sum_{j\neq i}\Omega_j$, we end up with the following analytical expressions for different temporal regimes:

$$\frac{1}{\mathcal{H}}\frac{\mathrm{d}\mathcal{H}}{\mathrm{d}x} \approx -\frac{\alpha_i}{2} = \begin{cases} -1 & \alpha_{\mathrm{rad}} = 2 \\ -\frac{1}{2} & \alpha_{\mathrm{M}} = 1 \\ 1 & \alpha_\Lambda = -2 \end{cases} \tag{25}$$

$$\frac{1}{\mathcal{H}}\frac{\mathrm{d}^2\mathcal{H}}{\mathrm{d}x^2} \approx \frac{\alpha_i^2}{4} = \begin{cases} 1 & \alpha_{\mathrm{rad}} = 2 \\ \frac{1}{4} & \alpha_{\mathrm{M}} = 1 \\ 1 & \alpha_\Lambda = -2 \end{cases} \tag{26}$$

$$\mathcal{H} \approx H_0\sqrt{\Omega_{i0}e^{-\alpha_i x}} = \begin{cases} H_0\sqrt{\Omega_{\mathrm{rad}0}}e^{-x} & \alpha_{\mathrm{rad}} = 2 \\ H_0\sqrt{\Omega_{\mathrm{M}0}}e^{-x/2} & \alpha_{\mathrm{M}} = 1 \\ H_0\sqrt{\Omega_{\Lambda 0}}e^{x} & \alpha_\Lambda = -2 \end{cases} \tag{27}$$

$$\frac{\eta\mathcal{H}}{c} \approx \begin{cases} 1 & \alpha_{\rm rad} = 2 \\ 2 & \alpha_{\rm M} = 1 \\ \infty & \alpha_\Lambda = -2 \end{cases} \tag{28}$$

These equations will be useful when making sure that the implementations are correct.[4] For a thorough derivation, see Appendix B.

### 2.2. Methods

We have to consider the time evolution of the density parameters, given some present value, as function of our chosen time parameter, here $x$. The density evolution is implemented as:

$$\Omega_n = e^{-\alpha_n x}\Omega_{n0}\mathcal{H}_{\rm rat}^2 \tag{29}$$

where we have defined the ratio $\mathcal{H}_{\rm rat} \equiv H_0/\mathcal{H}$, and the new index $n$ are all the densitis: $n \in \{b, \mathrm{CDM}, \gamma, \nu, \Lambda, k\}$.

We also implement functions to solve for the luminosity distance (Eq. (15)), angular distance (Eq. (14)), and the conformal distance (Eq. (12)).

#### 2.2.1. ODEs and Splines

The differential equations for $\eta$ (Eq. (16)) and $t$ (Eq. (17)) are solved numerically as ordinary differential equations with the Runge-Kutta 4 as advancement method. The equations are solved for $x \in (-20, 5)$. As initial condition we would like $\eta(-\infty)$ which is obviously not possible to calculate, so we pick some very early time and use the analytical approximation in the radiation dominated era (Eq. (28)), which yield:

$$\eta(x_0) = \frac{c}{\mathcal{H}(x_0)}. \tag{30}$$

Likewise for $t$, the initial condition is:

$$t(x_0) = \frac{1}{2H(x_0)}. \tag{31}$$

We then proceed by making splines of both $\eta$ and $t$ in order to evaluate accurately for any $x \in (-20, 5)$.

#### 2.2.2. Fit to supernova data

We make predictions of the luminosity distance at different redshifts $z$, according to the discussion in Section 2.1.2. These predictions are compared with real supernova observations, acquired by Betoule et al. (2014). In order to constrain the possible values of $h$, $\Omega_{\rm M}$ and $\Omega_\Lambda$ we find the $\chi^2$-value between the luminosity distance of the supernovas and our predictions. The $\Omega$-s are sampled with Markov-Chain Monte Carlo sampling using the Metropolis-Hastings algorithm.

The parameters in question are $\Theta = \{h, \Omega_{m0}, \Omega_{k0}\}$, and we denote the observed data $\mathcal{D}_i = d_L^{\rm obs}(z_i)$. We assume the likelihood that the observed data is true, follows a normal distribution, with the observed value as mean, and uncertainty as standard deviation. Mathematically: $P(\mathcal{D}_i|\Theta) \sim \mathcal{N}(\mathcal{D}_i, \sigma_i^2)$. The total likelihood is thus the product of all $N$ data points:

$$\mathcal{L}(\Theta|\mathcal{D}) = \prod_{i=1}^{N} P(\mathcal{D}_i|\Theta) \propto \exp\left\{-\frac{\chi^2}{2}\right\} \tag{32}$$

The last proportionality follows from the fact that $P$ is normally distributed and that we use:

$$\chi^2(\Theta) = \sum_{i=1}^{N} \frac{(d_L(z_i,\Theta) - \mathcal{D}_i)^2}{\sigma_i^2}. \tag{33}$$

We use as prior (the probability that the observed data are true without any further information), a uniform distribution that is 1 if the parameters are within the following ranges (0 otherwise): $0.5 < h < 1.5$, $0.0 < \Omega_{m0} < 1.0$, $-1.0 < \Omega_{k0} < 1.0$. These are the absolute ranges of the parameters. Thus, according to Bayes' theorem, within these ranges we have that the posterior probability

$$P(\Theta|\mathcal{D}) \propto \mathcal{L}(\Theta|\mathcal{D}) \cdot \mathrm{Prior} = \mathcal{L}(\Theta|\mathcal{D}). \tag{34}$$

Thus, finding the most probable set of parameters $\Theta$ is equivalent to find the set with the largest likelihood, which again is similar to finding the set which minimises $\chi^2$.

When performing MCMC sampling (with MH-algorithm), we use Eq. (32) as the likelihood function. That means that we would expect normally distributed values of the different parameters, $\Theta$. We may from the distributions of each parameter estimate the mean (true value) and a confidence interval from its standard deviation. We may also find the $1\sigma$ confidence space for the collection of parameters in $\Theta$, by considering the distribution of $\chi^2$. This is a famous distribution whose $1\sigma$ interval (for $k = 3$ degrees of freedom in this case) is given by $\left|\chi^2 - \chi^2_{\rm min}\right| < 3.53$.

It is also of interest to say something about whether the fit is any good at all. It is easy to see from Eq. (33) that if the difference between prediction and observation matches the uncertainties in the observed data, then we have $\chi^2 \simeq N$, which is the best fit we can hope for (since we fit to data which has an intrinsic uncertainty already). If $\chi^2 \ll N$, then we *over-fit* the model, while if $\chi^2 \gg N$ then we have an increasingly bad fit. In summary, we may analyse the following quantity

$$\frac{\chi^2}{N} \begin{cases} \ll & 1 \quad \text{over} - \text{fitting}, \\ \simeq & 1 \quad \text{good fit}, \\ \gg & 1 \quad \text{bad fit}, \end{cases} \tag{35}$$

in order to determine the goodness of fit.

### 2.3. Results and discussion

#### 2.3.1. Tests

Fig. 1 show the evolution of the density fractions with time. They sum to one across all times which was required. At early times the radiation density dominates (orange line). The intersection between the orange and green lines mark the radiation-matter equality, after which matter is the dominating density. Likewise, the intersection between the green and purple lines mark the matter-dark energy equality, where dark energy (manifested in the cosmological constant) become the dominating density. Time can thus be divided into three regimes; radiation dominated, matter dominated, and dark energy dominated eras, separated by black dotted lines in the plot.

[4] Eq. (28) is a bit hand-wavy as $\eta$ is really an integral, so assuming a dominant density parameter, means assuming it for the whole existence of the universe, not only the regime we are looking at. We may hence expect these to bee gradually more wrong as the Universe evolves. TODO: DO I HAVE TIME TO FIX THIS?

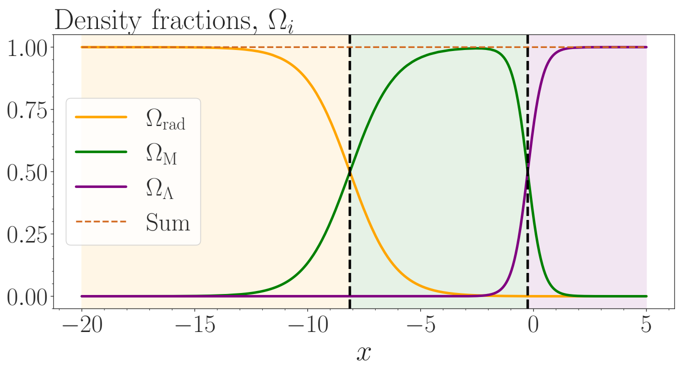


**Fig. 1.** Density fractions $\Omega_i$ as function of $x$. For low $x$, radiation dominates, before matter dominates and dark energy has just become the dominant energy density today $x = 0$, and will continue to dominate into the future. The sum of densities sums to one across all times, as required (white dotted line). The black dotted lines are the radiation-matter equality at $x = -8.13$ and the matter-dark energy equality at $x = -0.26$, both stated in Table 1. The domination of each regime is shown as a shaded background with similar colour as its respective graph.

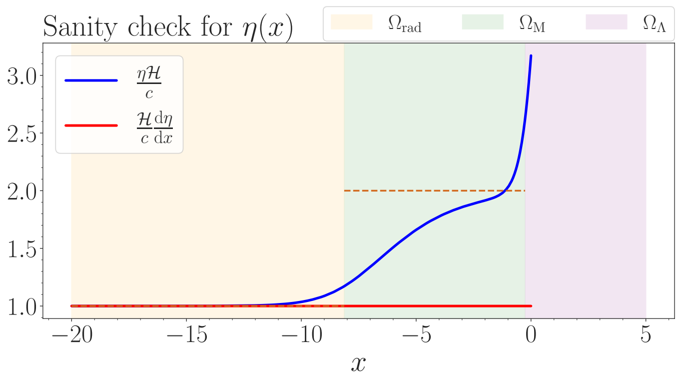


**Fig. 2.** Sanity check for $\eta$. $\eta\mathcal{H}/c$, in blue, is 1 in the radiation regime, 2 in the matter regime and diverging toward $+\infty$ in the dark energy regime, as expected from the analytical approximations in each regime. Remembering that this is strictly correct only in the radiation regime explains the mismatch of the brown doted line in the matter regime. $(d\eta/dx)\mathcal{H}/c$, in red, is 1 throughout time, as expected from Eq. (16).

TODO: fix this As explained in section Section 2.1.4, we have analytical solutions for constructions of $\eta$ and $\mathcal{H}$ in the different regimes. Fig. 2 is the sanity check for $\eta$, showing $\eta\mathcal{H}/c$ converging to finite values in the radiation and matter dominated eras (where $\alpha_{\rm rad,M} > 0$), and diverging towards $+\infty$ in the dark energy dominated era ($\alpha_\Lambda = -2 < 0$). This is in accordance with the analytical solutions. The different regimes are shown in shaded colour. It is also worth noticing that $(d\eta/dx)\mathcal{H}/c$ is one for all regimes, as expected from equation Eq. (16). TODO: to this

Fig. 3 is the sanity check confirming that our constructions of $\mathcal{H}$ and its derivatives converge to the analytical approximation in the different regimes. The second derivative, as shown in blue, takes the value of 1 in the radiation regime, 1/4 in the matter regime and 1 in the dark energy regime. Similarly, the first derivative, as shown in red, take the value -1 in the radiation regime, -1/2 in the matter regime and 1 in the dark energy regime. This is well in accordance with the analytical approximations put forth in section Section 2.1.4.

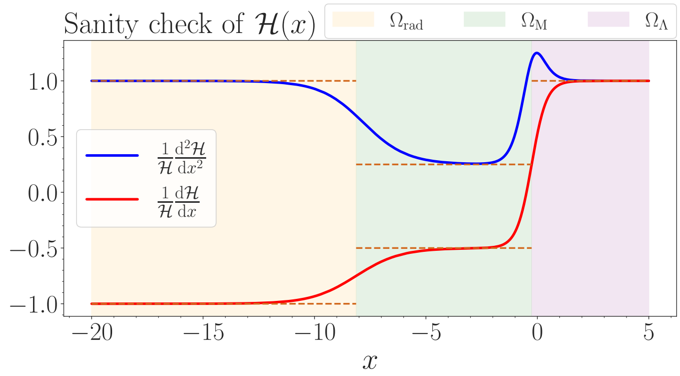


**Fig. 3.** Sanity check for $\mathcal{H}$, showing that the second derivative (blue) converge to the analytical expressions shown as brown dotted lines in the different regimes. The first derivative (red) converge to its analytical values in the same regimes, which again are shown with a shaded colour.

| Quantity | $x$ | $z$ | $t$ |
|---|---|---|---|
| RM-equality | -8.13 | 3400 | $51{\cdot}10^3$ yr |
| ML-equality | -0.26 | 0.29 | 10.378 Gyr |
| Accel. start | -0.49 | 0.63 | 7.752 Gyr |
| Age of universe | 0.00 | 0.00 | 13.858 Gyr |
| Conformal time | 0.00 | 0.00 | 46.319 Gyr |

**Table 1.** Important quantities in the evolution of the universe. RM stands for radiation-matter and ML for matter-dark energy.

These sanity checks are confirmations that the implementations yield the same result as the analytical approximation in the different regimes for various constructions of $\eta$ and $\mathcal{H}$ and their derivatives.

### 2.3.2. Analysis

In Section 2.1.3 we indicate how we can calculate the radiation-matter equality (RM-equality), matter-dark energy equality (ML-equality), when the acceleration of the universe started, the age of the universe and the conformal time today. The result is shown in Table 1. We note that the equalities is in accordance with the sanity checks, and the age of the universe today (in cosmic time) is about 13.9 Gyr. We also note that the acceleration onset is slightly before the matter-dark energy equality at $x = -0.49$ and $x = -0.26$ respectively.

The conformal Hubble factor, $\mathcal{H}$, is plotted against time, $x$, in Fig. 4. It is decreasing in the radiation and matter regimes and increasing in the dark energy regime, switching signs at the acceleration onset, which is marked with a black dotted line in the figure.

Fig. 5 show the cosmic time $t$ and the conformal time $\eta/c$. The cosmic time is the age of the universe at any given time/size $x$. The low values for the cosmic time at early times suggest a rapid increase of the size of the Universe in a short cosmic time. This is supported by the conformal Hubble factor in Fig. 4 which is large for low $x$. The expansion rate of the universe decelerates until the acceleration onset, from which it accelerates. TODO: explain $\eta$ and $t$ more

The results of the supernova fitting, outlined in section Section 2.2.2, is summarised in Table 2. The parameter values that maximises the likelihood (minimising) $\chi^2$ are: $h = 0.702$, $\Omega_{\rm M0} = 0.259$ and $\Omega_{k0} = 0.274$. We also compute the posterior probability distribution function obtained from Eq. (34) which

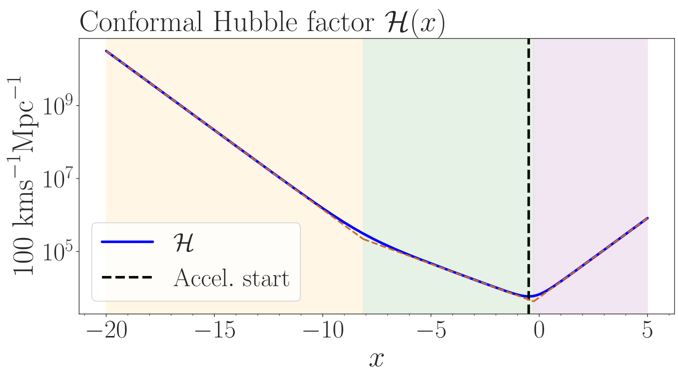


**Fig. 4.** $\mathcal{H}$ as function of $x$. It is decreasing in the radiation and matter regimes, and increasing in the dark energy regime, tightly following its analytical approximation in each regime.

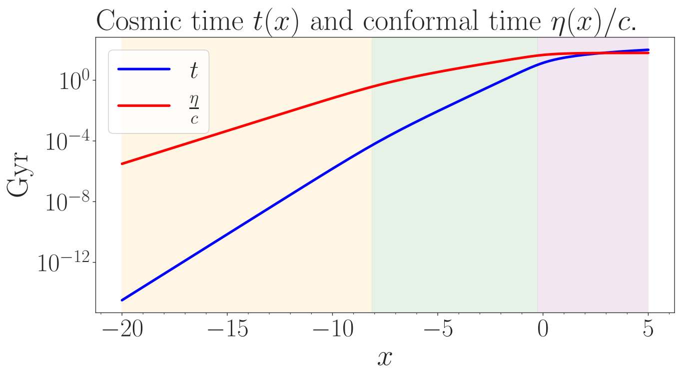


**Fig. 5.** Cosmic time (in blue) and conformal time (red). TODO: find meaning behind this plot.

| | $h$ | $\Omega_{\mathrm{M0}}$ | $\Omega_{k0}$ |
|---|---|---|---|
| Best: min $\chi^2$ | 0.702 | 0.259 | 0.067 |
| Posterior | 0.701 | 0.247 | 0.107 |
| $1\sigma$ confidence | 0.006 | 0.110 | 0.274 |

**Table 2.** Best and fitted values. The best fit values are those that actually minimise the $\chi^2$-value, which consequently are the most probable values. The fitted values are obtained as the mean and standard deviations of the posterior pdfs of the parameters respectively.

we have assumed to be normally distributed. From this we obtain a mean value, but also a $1\sigma$ confidence interval, which are:

$$\begin{aligned} h &= 0.701 \pm 0.006 \\ \Omega_{\mathrm{M0}} &= 0.247 \pm 0.110 \\ \Omega_{k0} &= 0.107 \pm 0.274 \end{aligned} \tag{36}$$

Let's first see for ourselves if these values make sense or not, just with by-eye comparison. Fig. 6 shows the supernova data as red error bars, with the predictions from the fiducial cosmology plotted above it, alongside the best fit parameter values. The quantity plotted is the luminosity distance divided by redshift, $d_L/z$ for better comparison. We notice the accordance between the two, and also note that the $x$-axis in this plot is the redshift $z$ instead of the logarithm of the scale factor. This means that earlier times are to the right in the plot (high redshift), as opposed to the other plots. Immediately we see that the best fit parameters seems to do a better job at staying within the red error bars. However, the fiducial cosmology is also quite good. Furthermore, the

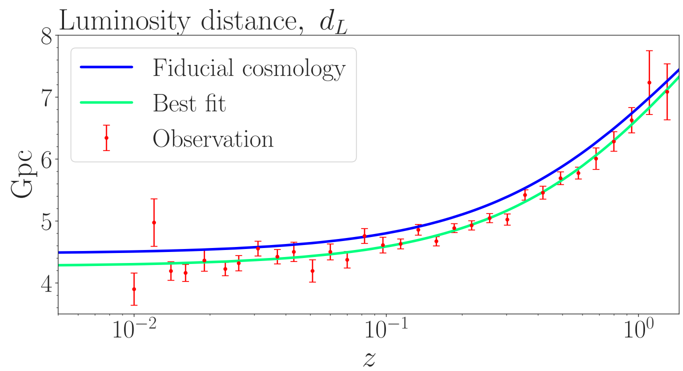


**Fig. 6.** The luminosity distance predicted using the fiducial cosmology in blue, against observations of actual supernovas in red (or rather the confidence interval of the observations). The green line is found from computing the luminosity distance using a cosmology of the best fit parameters from the supernova fitting; $h = 0.702, \Omega_{\mathrm{b0}} = 0.05, \Omega_{\mathrm{CDM0}} = 0.209, \Omega_{\mathrm{k}} = 0.067, N_{\mathrm{eff}} = 3.046, T_{\mathrm{CMB}} = 2.7255\mathrm{K}$. Notice the $x$-axis is now the redshift $z = e^x - 1$.

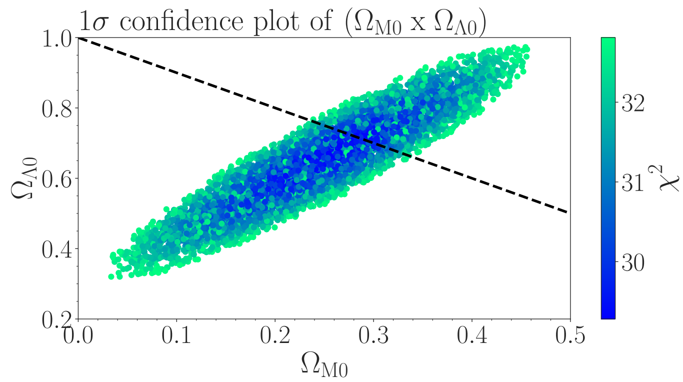


**Fig. 7.** Scatter plot showing the $\chi^2$-values of the luminosity distance $d_L$ between the observed values $\mathcal{D}$ and the sampled values, as function of $\Omega_{\mathrm{M0}}$ and $\Omega_{\Lambda0}$. The data shown is the $1\sigma$ confidence region. The black dotted line signifies a flat universe.

fiducal cosmology stays well within the $1\sigma$ confidence interval found from the posterior pdfs. It is also worth noting that the uncertainties on some observed values are quite large.

Now let's turn to how we have constrained the parameters. Fig. 7 shows the $\chi^2$-values found from Eq. (33), constrained to $1\sigma$ interval. The black dotted line represent a flat universe, where the matter and dark energy are the main constituents of the universe. The supernova data originate in close temporal proximity to us, we thus assume that the contribution from the radiation density is negligible for making constraints on $\Omega_{\mathrm{M0}}$ and $\Omega_{\Lambda0}$ today. Having only $\Omega_{\mathrm{M0}}$, $\Omega_{\Lambda0}$ and $\Omega_{k0}$, where only two of them are free yield: $\Omega_{k0} = 1 - (\Omega_{\mathrm{M0}} + \Omega_{\Lambda0})$, which fixes the relationship, so that it does not really matter which two of them we constrain, as the constraint on the third automatically follows.[5]

From the sampled values we then generate the posterior pdf by making a histogram of all the samples. This is seen for $\Omega_{\mathrm{M0}}$ and $\Omega_{k0}$ in Fig. 8 and for $H_0$ in Fig. 9, all histograms are in turquoise. From the samples we also find their respective mean and standard deviation, from which we plot a green Gaussian curve on top of the histogram. The means are indicated with black dotted lines, and the $1\sigma$ confidence regions are shaded in

[5] This is why we are able to put constraints on $\Omega_{\Lambda0}$ even though this parameter is not (directly) sampled in the MCMC sampling.

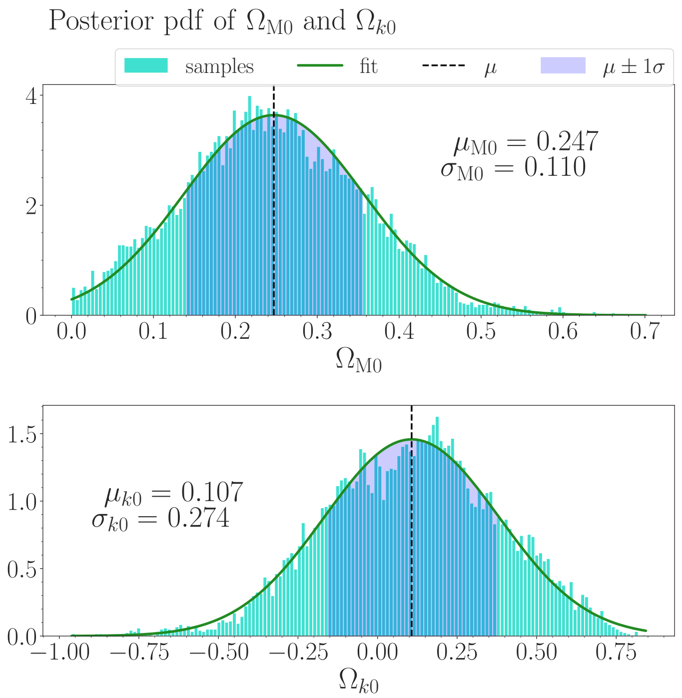


**Fig. 8.** Posterior probability distributions (pdfs) of $\Omega_{M0}$ and $\Omega_{k0}$ as result of the MCMC sampling. The samples are shown in turquoise and the constructed pdfs in green. The mean $\mu$ is shown as a black dotted line, with the $1\sigma$ confidence interval in shaded blue ($\mu \pm 1\sigma$)

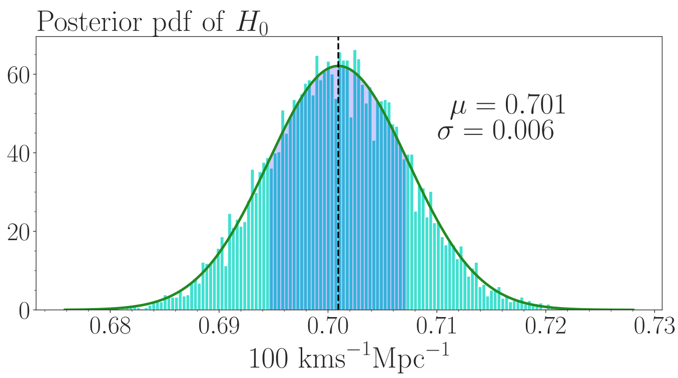


**Fig. 9.** Posterior probability distribution (pdf) of $H_0$ as result of the MCMC sampling.

blue. Both quantities are also stated in text in each plot, inn accordance with those presented in Table 2. From inspection, we see that the histograms are quite close to being normally distributed, so the fitted Gaussian is quite a good fit.

Discussing the goodness of the fit further, we may turn to the criterion from Eq. (35). Fig. 10 show a histogram of the sampled $\chi^2$ values, divided by $N$. In sight of prior discussion, the mean value of $\chi^2/N$ is 1.052, which is not that much larger than 1. Thus, we deduce that the fit is quite good. Although we also see from the figure that $\chi^2/N$ deviates significantly from the Gaussian curve in green.

Nevertheless, we shall continue to use the fiducial cosmology from Betoule et al. (2014), but now we have some viable constraints on them.

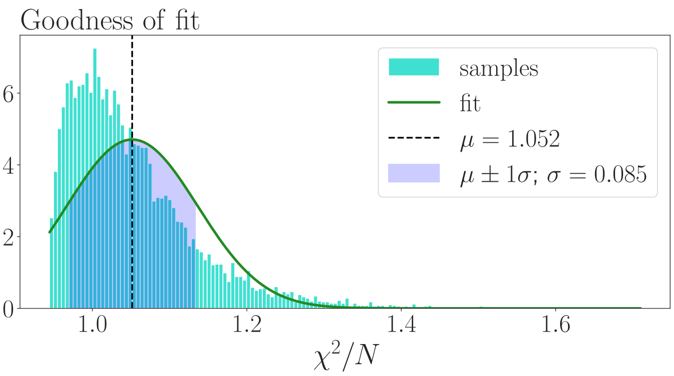


**Fig. 10.** Goodness of fit, showing the mean value of $\chi^2/N$ is close to 1, which is a good fit. The Gaussian function does not seem to encapsulate behaviour of the samples. TODO: is it really a $\chi^2$-distribution with 3 dof?. hmmm.

## 3. Milestone II - Recombination History

The main goal of this section is to investigate the recombination history of the universe. This can be explained as the point in time when photons decouple from the equilibrium of the opaque, early universe. When this happens, photons scatter for the last time at the *time of last scattering*, and these photons are what we today observe as the CMB. This period of the history of the universe is thus crucial for understanding the CMB.

We will start by calculating the free *electron fraction* $X_e$, from which we may find the *optical depth* $\tau$. This again enables us to compute the *visibility function*, $g$, and the *sound horizon*, $s$. The latter will be of great importance later.

Recombination happens because the expansion of the Universe cools it down, making the photons less energetic, which in turn make each interaction in the primordial plasma less energetic. At some point, hydrogen atoms are able to form, reducing the number of free electron, hence reducing photon interactions, until they scatter for the last time. We will determine the time of recombination from the free electron fraction, which indirectly tell us how large portion of the free electron have (re)-combined.[6] Due to the decrease of free electron, photons interact less with them (optical depth is decreased). At some point, photons scatter for the last time, and this information is encapsulated in the visibility function.

### 3.1. Theory

In order to explain the inventory of the universe, we need to understand how the distribution of different species changes over time. This is governed by the *Boltzmann equation*,

$$\frac{\mathrm{d}f}{\mathrm{d}t} = C[f], \tag{37}$$

where $f(\mathbf{x}, \mathbf{p}, t)$[7] is the distribution function of a given species. $C[f]$ are the collision terms, which depends on the species through the same distribution function $f$. Due to the function dependencies of $f$ we are able to generally expand it into (Dodelson & Schmidt 2020, Eq. 3.33):

$$\frac{\mathrm{d}f}{\mathrm{d}t} = \frac{\partial f}{\partial t} + \frac{\partial f}{\partial x^i}\frac{\mathrm{d}x^i}{\mathrm{d}t} + \frac{\partial f}{\partial p}\frac{\mathrm{d}p}{\mathrm{d}t} + \frac{\partial f}{\partial \hat{p}^i}\frac{\mathrm{d}\hat{p}^i}{\mathrm{d}t} = C[f], \tag{38}$$

[6] As with any good article on the subject, we ought to say that recombination is a funny wording, as this is the first time in the history of the Universe that protons and electrons combine to form hydrogen.

[7] Given in *phase-space coordinates*: $(x^\mu, P^\mu)$

where $p = |\mathbf{p}|$ and $\hat{p} = \mathbf{p}/p$.

Before recombination, the equilibrium between protons, electrons and photons is governed by the following interaction, from Weinberg (2008)[8]:

$$e^- + p^+ \leftrightharpoons H^* + \gamma, \tag{39}$$

where a proton and an electron interact to form an excited hydrogen atom, which decays and emits a photon, or a photon excites and split a hydrogen atom into a free electron and a proton through *Compton scattering*.[9] Eq. (39) is a reaction of the form $1 + 2 \leftrightharpoons 3 + 4$, and we have from Winther et al. (2023) that the Boltzmann equation for such a reaction is:

$$\frac{1}{n_1 e^{3x}} \frac{\mathrm{d}(n_1 e^{3x})}{\mathrm{d}x} = -\frac{\Gamma}{H}\left(1 - \frac{n_3 n_4}{n_1 n_2}\left(\frac{n_1 n_2}{n_3 n_4}\right)_{\mathrm{eq}}\right), \tag{40}$$

where $n_i$ are the number densities of the reactants, $\Gamma$ is the reaction rate and $H$ the Hubble parameter (expansion rate of the universe). If the reaction rate is much larger than the expansion rate of the universe, $\Gamma \gg H$, then Eq. (39) ensures equilibrium between protons, electron and photons. When $\Gamma$ drops below $H$, then the expansion rate becomes dominant and the reaction rate is unable to sustain equilibrium. This happens when the temperature of the Universe becomes lower than the binding energy of hydrogen, hence stable neutral hydrogen is able to form.[10] As a consequence, the photons *decouple* from the protons and electron. When $\Gamma \ll H$, there are practically no interactions and the number density becomes constant for a comoving volume. Massive particles *freeze out* and their abundance become constant.

#### 3.1.1. Hydrogen recombination

We express the electron density through the free electron fraction $X_e \equiv n_e/n_{\mathrm{H}} = n_e/n_b$ where we have assumed that hydrogen make up all the baryons ($n_b = n_{\mathrm{H}}$). We also ignore the difference between free protons and neutral hydrogen. From Callin (2006) we obtain:

$$n_b = \frac{\rho_b}{m_{\mathrm{H}}} = \frac{\Omega_b \rho_c}{m_{\mathrm{H}}} e^{-3x}, \tag{41}$$

where $m_{\mathrm{H}}$ is the mass of the hydrogen atom, and $\rho_c$ the critical density today as defined earlier. Before recombination, no stable neutral hydrogen is formed, thus the electron and baryon density is the same, i.e. there are only free electrons so $X_e \simeq 1$. When in equilibrium, the r.h.s. of Eq. (40) reduces to 0, which is called the *Saha approximation*. The solution is in this regime described by the *Saha equation*, which from Dodelson & Schmidt (2020) in physical units is:

$$\frac{X_e^2}{1 - X_e} = \frac{1}{n_b}\left(\frac{k_B m_e T_b}{2\pi\hbar^2}\right)^{3/2} e^{-\epsilon_0/k_B T_b}, \tag{42}$$

where $\epsilon_0 = 13.6\,\mathrm{eV}$ is the ionisation energy of hydrogen. The Saha equation is only a good approximation when $X_e \simeq 1$. Thus for $X_e < (1 - \xi)$,[11] which corresponds to the period during and after recombination, we have to make use of the more accurate *Peebles equation*. From Callin (2006):

$$\frac{\mathrm{d}X_e}{\mathrm{d}x} = \frac{C_r(T_b)}{H}\left[\beta(T_b)(1 - X_e) - n_{\mathrm{H}}\alpha^{(2)}(T_b)X_e^2\right], \tag{43}$$

where

$$C_r(T_b) = \frac{\Lambda_{2s-1s} + \Lambda_\alpha}{\Lambda_{2s-1s} + \Lambda_\alpha + \beta^{(2)}(T_b)}, \tag{43a}$$

$$\Lambda_{2s-1s} = 8.227\ \mathrm{s}^{-1}, \tag{43b}$$

$$\Lambda_\alpha = \frac{1}{(\hbar c)^3} H \frac{(3\epsilon_0)^3}{(8\pi)^2 n_{1s}}, \tag{43c}$$

$$n_{1s} = (1 - X_e) n_{\mathrm{H}}, \tag{43d}$$

$$n_{\mathrm{H}} = (1 - Y_p)\frac{3H_0^2 \Omega_{b0}}{8\pi G m_{\mathrm{H}}} e^{-3x}, \tag{43e}$$

$$\beta^{(2)}(T_b) = \beta(T_b) e^{3\epsilon_0/4k_B T_b}, \tag{43f}$$

$$\beta(T_b) = \alpha^{(2)}(T_b)\left(\frac{k_B m_e T_b}{2\pi\hbar^2}\right)^{3/2} e^{-\epsilon_0/k_B T_b}, \tag{43g}$$

$$\alpha^{(2)}(T_b) = \frac{\hbar^2}{c}\frac{64\pi}{\sqrt{27\pi}}\frac{\alpha^2}{m_e^2}\sqrt{\frac{\epsilon_0}{k_B T_b}}\phi_2(T_b), \tag{43h}$$

$$\phi_2(T_b) = 0.448 \ln\left(\frac{\epsilon_0}{k_B T_b}\right). \tag{43i}$$

The Peebles equation takes into account that the energy (excitation) of hydrogen formed through Eq. (39) vary, and that decays take place until we reach the $n = 2$ level (first excited state), denoted by $^{(2)}$ in Eq. (43a)- Eq. (43i). Recombination to the ground state is not relevant, as this leads to an ionised photon which immediately ionises a neutral hydrogen atom (Dodelson & Schmidt 2020, p. 97). The $C_r$ is the probability that singly ionised hydrogen is reionised further, where $\beta^{(2)}$ and $\beta$ are the collisional ionisations from the first ionised state and ground state respectively. $\alpha^{(2)}$ is the recombination rate to excited states. For more detailed description of these terms, see Ma & Bertschinger (1995). [12]

We find $X_e$ by solving Eq. (42) for $X_e > (1-\xi)$ and Eq. (43) for $X_e < (1-\xi)$. In theory, it is possible to solve the Peebles equation at very early times, but the equation is very stiff resulting in unstable numerical solutions at early times (high temperatures), hence the Saha approximation.

[8] Where $H^*$ denotes excited states of hydrogen which will decay into neutral hydrogen.

[9] Elastic scattering of photons is technically Thomson scattering, but Compton scattering is a more general term and will be used ( Dodelson & Schmidt (2020)). This is also why we later use the Thomson cross section $\sigma_T$. The reaction is when a photon scatters of an electron, and possibly energises it enough to break out of the hydrogen atom, if already bound:

$$\gamma + e^- \leftrightharpoons \gamma + e^-.$$

[10] Well, it is really not as simple, as neutral hydrogen is obtained from excited hydrogen and how this process go about is non-trivial. As we ignore re-ionisation, I will not delve into this. However, both (Weinberg 2008, p. 113-129), (Dodelson & Schmidt 2020, p. 95-99) and Winther et al. (2023) elaborate further on this.

[11] Where $\xi$ is some small tolerance, which have to be defined in some numerical model for when to abonden the Saha equation and use the more accurate, but computationally more expensive Peebles equation. This is typically $\xi = 0.001$

[12] Because of this non-trivial path into the ground state, and the large photon to baryon number ratio, recombination happens later than when the temperature of the universe correspond to exactly the binding energy of neutral hydrogen ( Callin (2006))

#### 3.1.2. Visibility

Visibility is a concept tied to the optical depth and mean free path of a medium. The two latter are inversely proportional to each other. The mean free path is the average distance a photon travels before its direction is changed (often by scattering). Thus, a small mean free path gives results in a lot of collision across short distances, which occurs in optically thick media. The optical depth as a function of conformal time is defined as Winther et al. (2023):

$$\tau = \int_{\eta}^{\eta_0} n_e \sigma_{\rm T} e^{-x} d\eta', \tag{44}$$

where $n_e$ is the electron density and $\sigma_{\rm T}$ is the Thompson cross-section. In differential form, restoring original units, this is:

$$\frac{d\tau}{dx} = -\frac{c n_e \sigma_T e^x}{\mathcal{H}}. \tag{45}$$

From this we define the visibility function, $g$:

$$g = -\frac{d\tau}{d\eta} e^{-\tau} = -\mathcal{H} \frac{d\tau}{dx} e^{-\tau}$$
$$\tilde{g} \equiv -\frac{d\tau}{dx} e^{-\tau} = \frac{g}{\mathcal{H}}, \tag{46}$$

where $\tilde{g}$ is in terms of the preferred time variable, $x$. Notable thing about the visibility function $\tilde{g}$ is that it is a true probability distribution, describing the probability density of some photon to last have scattered at time $x$. Because of this, we have that $\int_{-\infty}^{0} \tilde{g}(x) dx = 1$. We also take note of the derivative of the visibility function:

$$\frac{d\tilde{g}}{dx} = e^{-\tau} \left[ \left( \frac{d\tau}{dx} \right)^2 - \frac{d^2\tau}{dx^2} \right] \tag{47}$$

#### 3.1.3. Sound horizon

Let's take a small step back and consider the situation of the early Universe. Before any decoupling, the photons and electrons are coupled through Thompson scattering, and protons and electrons are coupled through coulomb interactions. Because of this, photons interact with baryons and move alongside with them as one fluid, in which wave propagates with a speed $c_s$, from Dodelson & Schmidt (2020):

$$c_s \equiv c \left[ 3(1+R) \right]^{-\frac{1}{2}} \quad ; \quad R \equiv \frac{3\Omega_b}{4\Omega_\gamma}, \tag{48}$$

where $R$ is the *baryon-to-photon energy ratio*. By the definition of $R$, if the baryon density is negligible compared to the radiation density, $R \sim 0$, and we recover the wave propagation speed in a relativistic fluid: $c_s = 3^{-1/2}$ ( Dodelson & Schmidt (2020)). The total distance such a wave would have travelled in a time $t$ (since the beginning of the Universe) is called the *sound horizon*, found by simply integrating $c_s$ through time, accounting for the expansion of space itself by including a factor $e^{-x}$:

$$s = \int_0^t c_s e^{-x} dt = \int_{-\infty}^{x} \frac{c_s}{\mathcal{H}} dx, \tag{49}$$

where the variables are changed to $x$. On differential form:

$$\frac{ds}{dx} = \frac{c_s}{\mathcal{H}}, \tag{50}$$

which is a straightforward differential equation to solve given some initial conditions.

### 3.2. Methods

#### 3.2.1. Computing $X_e$

First things first, we need to compute the free electron fraction $X_e$. We are for the most part not interested in things happening in the future here, so the temporal range of choice will be $x \in [-20, 0)$ where $x = 0$ is today, and $x = -20$ is sufficiently long ago, so that the range encapsulated effect studied here. In the early Universe, the energies are so high that all baryonic matter is in the form of free electron, $X_e \simeq 1$, so we will start by solving the Saha equation, Eq. (42). We continue to solve equation Eq. (42) as long as $X_e > 1 - \xi$ where we use $\xi = 0.01$.

If we define:

$$K \equiv \frac{1}{n_b} \left( \frac{k_B m_e T_b}{2\pi\hbar^2} \right)^{3/2} e^{-\epsilon_0/k_B T_b}, \tag{51}$$

then equaton Eq. (42) takes the form $X_e^2 + K X_e - K = 0$, which is solved as a normal quadratic equation[13], where $a = 1$, $b = K$ and $c = -K$. Since $0 \le X_e \le 1$ we choose the positive solution, given by:

$$X_e = \frac{-K + \sqrt{K^2 + 4K}}{2} = \frac{K}{2} \left( -1 + \sqrt{1 + 4K^{-1}} \right) \tag{52}$$

This solution has the potential to become numerically unstable if the parenthesis is close to zero, i.e. for $K \gg 1$. We then make use of the approximation $\sqrt{1 + 4K^{-1}} \approx 1 + (2K^{-1})$ for $|4K^{-1}| \ll 1$, which ensures $X_e \simeq 1$ for very high temperatures (large $K$).

We continue to solve the Peebles equation as stated in Eq. (43), where the r.h.s. is implemented sequentially as Eq. (43a)- Eq. (43i) in reverse order. The initial condition is the last computed electron fraction above the cut-off: $X_{e0} = \min(X_e > 1 - \xi)$ as found from the Saha equation. It is solved for the x-range not solved by the Saha equation. On thing to notice is that for late time, $T_b$ becomes small, meaning that $e^{\epsilon_0/k_B T_b}$ becomes enormous. This term is found in Eq. (43f), and we solve it by setting $\beta^{(2)}(T_b) = 2$ if $\epsilon/k_B T_b > 200$, in order to avoid overflow.

Having found $X_e$ for the entire x-range, we compute $n_e$ and spline both results.

#### 3.2.2. Computing $\tau$ and $\tilde{g}$

With $n_e$ we are able to solve the optical depth as defined in Eq. (45). The inital condition for this equation is that the optical depth today is zero: $\tau(x = 0) = 0$, meaning we have to solve this backwards in time. This is done by using the negative differential:

$$\frac{d\tau_{\rm rev}}{dx_{\rm rev}} = -\frac{d\tau}{dx} = \frac{c n_e \sigma_T e^x}{\mathcal{H}}, \tag{53}$$

and solving for positive $x_{\rm rev}$: $x_{\rm rev} \in [0, 20]$. In order to undo this reversal, we map $\tau = -\tau_{\rm rev}$ to its corresponding $x = -x_{\rm rev}$. Having found $\tau$, we find its derivative by solving equation Eq. (45), and further the find the visibility function from Eq. (46) and its derivative from Eq. (47). We ensure that $\int_{-\infty}^{0} \tilde{g} dx = 1$ as a

[13] $ay^2 + by + c = 0$ has solutions

$$y = \frac{-b \pm \sqrt{b^2 - 4ac}}{2}.$$

| Phenomenon | $x$ | $z$ | $t$ [Myr] | $r_s$ [Mpc] |
|---|---|---|---|---|
| Last scattering | -6.9853 | 1079.67 | 0.3780 | 145.31 |
| Recombination | -6.9855 | 1079.83 | 0.3779 | 145.29 |
| Saha | -7.1404 | 1260.89 | 0.2909 | 131.03 |

**Table 3.** The times of last scattering and recombination given in terms of $x$, the redshift $z$, the cosmic time $t$ and the sound horizon $r_s$. Also included is the time of recombination found using the Saha approximation only.

sanity check. All of these four quantities are splined, and their derivatives are obtained numerically.

In order to solve equation Eq. (49) for the sound horizon, we choose initial conditions $s_i = c_{s,i}/\mathcal{H}_i$ where the subscript $i$ denote a very early time (in our case when $x = -20$). We are then able to solve the differential equation for the sound horizon, Eq. (50), numerically and then spline the result.

#### 3.2.3. Analysis

Having splines for the relevant quantities enables us to compute some important times in the early universe. Firstly, the *last scattering surface*, is the time when most photons scattered for the last time, and decoupled from the plasma. This is not expected to have happened instantly, but recalling that the visibility function $\tilde{g}$ is a probability distribution function for when photons last scattered, we simply use the peak of this function as the definition of the last scattering surface.

Further, we want to find a time for when recombination happened, i.e. when free electron was captured by protons to form hydrogen atoms. Thus, this coincides with the reduction of the free electron fraction, and we will use $X_e = 0.1$ as the definition for when recombination happened. These numbers can also be computed using only the Saha approximation, for comparison. We also compute the sound horizon at these decouplings: $r_s = s(x_{\rm dec})$.

The last thing we want to compute is the freeze out abundance of free electrons, i.e. the free electron abundance today, which is found by evaluating the spline for $X_e$ at $x = 0$.

### 3.3. Results and discussion

#### 3.3.1. Times and sound horizon

The relevant times for last scattering, recombination and Saha recombination are obtained as explained in Section 3.2.3, and presented in Section 3.3.1. These times are given in terms of $x$, the redshift $z$ and the cosmic time $t$ (in Myr). The sound horizon is given in units of megaparsecs (Mpc). Last scattering occurred when $x = -6.9853$, at redshift $z = 1079.67$, which is slightly after recombination when $x = -6.9855$ at redshift $z = 1079.83$. If the Saha approximation was valid when the electron fraction dropped, recombination would have happened when $x = -7.1404$ at redshift 1260.89 which is significantly earlier. However, this is not the case since photons drop out of equilibrium with the primordial plasma as soon as hydrogen begin to form, and the free electron fraction is reduced. Thus, this number may only be used for comparison. Another thing worth noting is the validity of these numbers.

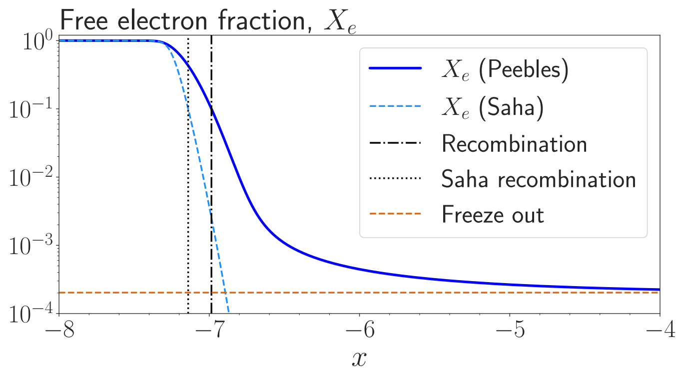


**Fig. 11.** The free electron fraction $X_e$ as function of $x$, found from the Saha and Peebles equation (blue). The result using only the Saha equation is shown in dashed light blue. The time of recombination is shown as a dashed black line. Likewise, recombination in the Saha approximation is shown as a dotted black line, appearing earlier. The freeze out abundance of hydrogen (the present value) is shown as a brown dashed line.

#### 3.3.2. Free electron fraction

Fig. 11 shows the free electron fraction $X_e$ as a function of $x$ found using both the Saha and Peebles equation, as explained in Section 3.2.1, in blue. Also shown is the results found from the Saha equation only, which tends to zero a lot faster. This is used for comparison only, as we have already stated that the Saha approximation is only valid for $X_e \simeq 1$. The time of recombination is shown for both cases, which for the Saha approximation happens significantly earlier than what is the actual case. The Peebles solution falls off gradually, and converges towards a constant value, which is the present day abundance of free electrons (freeze out abundance). This is found to be $X_e(x = 0) = 0.0002$, shown as a brown dashed line in Fig. 11.

Since the Peebles equation is a solution of the Boltzmann equation, it takes into account the particle interaction with changing abundance, after the photons decouple from the primordial plasma. It is thus expected that this will result in a much more gradual fall off of the free electron fraction, just as we observe in Fig. 11.

#### 3.3.3. Visibility

Fig. 12 shows the optical depth and its first two derivatives as functions of $x$. The surface of last scattering is shown with a black dashed line, before which the primordial plasma is optically thick, meaning the photons have a short mean free path. The decrease of the optical depth means that the photons gradually travel longer distances before interacting with free electrons. There are two processes going on here; the expansion of space itself, and the formation of neutral hydrogen. Both of which contribute to the increased mean free path of the photons. The contribution from the expansion of space is slow compared to the seemingly rapid change in the free electron fraction once neutral hydrogen is able to form. Thus, the rapid decrease of free electrons, as seen is Fig. 11 makes the mean free paths of photon to increase beyond the horizon. This effectively enable them to travel through space without interacting with matter, and this is what we observe as the CMB today - the Universe becomes transparent. This sudden decrease of optical depth is clearly seen in Fig. 12, both in $\tau$ itself, but also in its derivatives.

Another way of arriving at similar conclusions is by considering the visibility function in Fig. 13. Here, $\tilde{g}$ is shown in

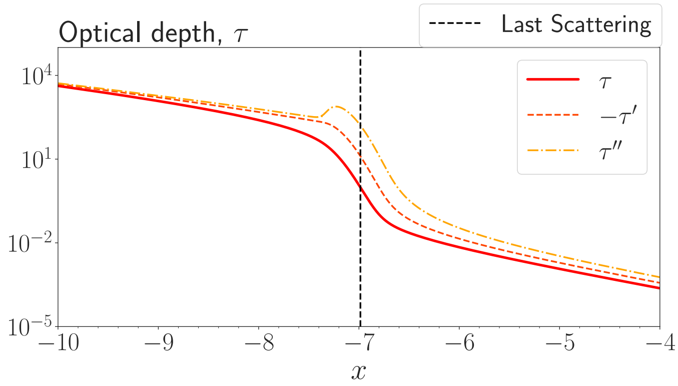


**Fig. 12.** The optical depth $\tau$ and its first and second derivatives as functions of $x$. The time of last scattering is shown as a dashed black line, before which the Universe was optically thick.

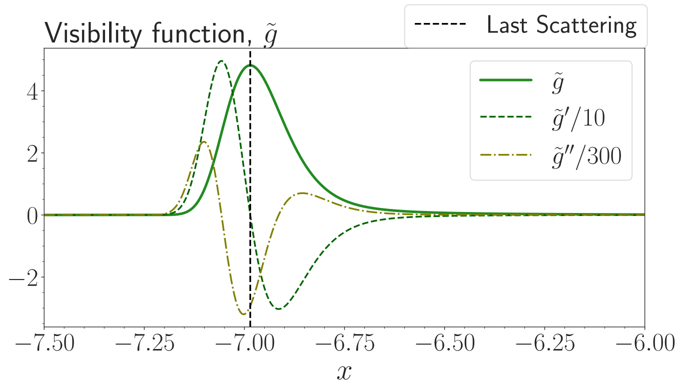


**Fig. 13.** The visibility function $\tilde{g}$ and its first and second derivatives as functions of $x$. The time of last scattering is shown as a dashed black line, which by definition coincides with the peak of the visibility function.

green along with its derivatives. The scaling follow that of Callin (2006), in order to fit the graphs into the same figure. $\tilde{g}$ describes the probability that a photon reaching us today scattered at time $x$. The peak of this function indicates the time were *the most* photons scattered for the last time, and is thus used as a definition of the last scattering surface. The visibility function is skewed forward in time. TODO: why?

#### 3.3.4. General discussion

One key thing to keep in mind is that recombination did not happen instantaneously, but rather over a relatively short period in which neutral hydrogen formed rapidly. This caused a rapid decrease of the free electron fraction, which again caused the optical depth to decrease by several magnitudes. In the same period, we see a that the visibility function is non-zero, meaning the probability of last scattering is (relatively) very high in this period. The times quoted in Section 3.3.1 are times that arise from our quite rigid, but fair definition of last scattering and recombination. However, these times do not encapsulate the duration of the abovementioned period. One could also define the last scattering surface as the time when $\tau = 1$ which is the transition between optically thick and optically thin media (when the photon travels exactly one mean free path before scattering). However, the visibility function is arguably a better choice since this is a proper probability distribution, so its peak represents the *actual* time when the probability of last scattering was the highest. Nevertheless, if we change these definitions we ought to expect different times as a result.

## 4. Milestone III - Perturbations

The aim of this section is to investigate how small fluctuations in the baryon-photon-dark-matter fluid in the early grew into larger structures. This is done by examining the interplay between these fluid fluctuations and the subsequent fluctuations of the space-time geometry. We will model this by perturbing the flat FLRW-metric using the conformal-Newtonian gauge. This will impact how the Boltzmann equations for the different species behaves, from which we are able to construct differential equations for key physical observables, and their initial conditions.

### 4.1. Theory

#### 4.1.1. Metric perturbations

The perturbed metric in the conformal-Newtonian gauge is given in Callin (2006) as:

$$g_{\mu\nu} = \begin{pmatrix} -(1+2\Psi) & 0 \\ 0 & e^{2x}\delta_{ij}(1+2\Phi) \end{pmatrix} \tag{54}$$

This means that we perturb the FLRW-metric with $\Psi \ll 1$ corresponding to the Newtonian potential governing the motion of non-relativistic particles and $\Phi \ll 1$ governing the perturbation of the spatial curvature. [14] The comoving momentum in this spacetime is:

$$P^{\mu} = \left[E(1-\Psi), p^i \frac{1-\Phi}{a}\right]. \tag{55}$$

By considering this momentum, and the geodesic equation in this perturbed spacetime we obtain the following (Dodelson & Schmidt 2020, Eqs. 3.62, 3.69, 3.71):

$$\frac{\mathrm{d}x^i}{\mathrm{d}t} = \frac{\hat{p}^i}{a}\frac{p}{E}(1-\Phi+\Psi) \tag{56a}$$

$$\frac{\mathrm{d}p^i}{\mathrm{d}t} = -\left(H + \frac{\mathrm{d}\Phi}{\mathrm{d}t}\right)p^i - \frac{E}{a}\frac{\partial\Phi}{\partial x^i} - \frac{1}{a}\frac{p^i}{E}p^k\frac{\partial\Phi}{\partial x^k} + \frac{p^2}{aE}\frac{\partial\Phi}{\partial x^i} \tag{56b}$$

$$\frac{\mathrm{d}p}{\mathrm{d}t} = -\left(H + \frac{\mathrm{d}\Phi}{\mathrm{d}t}\right)p - \frac{E}{a}\hat{p}^i\frac{\partial\Psi}{\partial x^i} \tag{56c}$$

Inserting Eq. (56) into Eq. (38), and for now assuming $C[f] = 0$ yield the *collisionless Bolzmann equations*. Keeping terms to first order only,[15] yield the collisionless Bolzmann equation: (Dodelson & Schmidt 2020, Eq. 3.83):

$$\frac{\mathrm{d}f}{\mathrm{d}t} = \frac{\partial f}{\partial t} + \frac{p}{E}\frac{\hat{p}^i}{a}\frac{\partial f}{\partial x^i} - \left[H + \frac{\mathrm{d}\Phi}{\mathrm{d}t} + \frac{E}{ap}\hat{p}^i\frac{\partial\Psi}{\partial x^i}\right]p\frac{\partial f}{\partial p}. \tag{57}$$

Future work consists mainly of evaluating the collision terms for each species and equate it to Eq. (57)

[14] $\Phi$ may also be interpreted as a *local perturbation to the scale factor*, Dodelson & Schmidt (2020).

[15] This is justified by the ansatz that deviations away from the equilibrium distribution of radiation in the inhomogeneous universe are of same order as the spacetime perturbations $\Phi$ and $\Psi$, Dodelson & Schmidt (2020).

#### 4.1.2. Fourier space and multipole expansion

Consider a function $f(\mathbf{x}, t)$. Its Fourier transform $\mathscr{F}$ and inverse $\mathscr{F}^{-1}$ are defined as:

$$\mathscr{F}[f(\mathbf{x}, t)] \equiv \frac{1}{(2\pi)^{3/2}} \int e^{-i\mathbf{k}\cdot\mathbf{x}} f(\mathbf{x}, t) \mathrm{d}^3 x = \tilde{f}(\mathbf{k}, t), \tag{58}$$

$$\mathscr{F}^{-1}[\tilde{f}(\mathbf{k}, t)] \equiv \frac{1}{(2\pi)^{3/2}} \int e^{i\mathbf{k}\cdot\mathbf{x}} \tilde{f}(\mathbf{k}, t) \mathrm{d}^3 k = f(\mathbf{x}, t). \tag{59}$$

It becomes apparent from these definitions that taking the spatial derivative with respect to $\mathbf{x}$ in real space, is the same as multiplying the function with $i\mathbf{k}$ in Fourier space. This leads to the following property: $\mathscr{F}[\nabla f(\mathbf{x}, t)] = i\mathbf{k}\mathscr{F}[f(\mathbf{x}, t)]$. This is of major significance when working with partial differential equations (PDEs), where:

$$\begin{aligned}
&\mathscr{F}[\nabla^2 f(\mathbf{x}, t)] = i^2 \mathbf{k} \cdot \mathbf{k} \mathscr{F}[f(\mathbf{x}, t)] = -k^2 \mathscr{F}[f(\mathbf{x}, t)] \\
&\mathscr{F}\left[\frac{\mathrm{d}^n f(\mathbf{x}, t)}{\mathrm{d}t^n}\right] = \frac{\mathrm{d}^n}{\mathrm{d}t^n} \mathscr{F}[f(\mathbf{x}, t)].
\end{aligned} \tag{60}$$

The two equations in Eq. (60) have the ability of reducing PDEs down to a set of decoupled ODEs. This means that we are able to solve for each mode $k = |\mathbf{k}|$ independently, which will be of great impact for the equations to come.

We will also work with multipole expansions, which are series written as sums of *Legendre polynomials* expanded in $\mu = \cos\theta \in [-1, 1]$ as:

$$f(\mu) = \sum_{l=0}^{\infty} \frac{2l+1}{i^l} f_l \mathcal{P}_l(\mu), \tag{61}$$

where $\mathcal{P}_l$ is the $l$-th Legendre polynomial. These are orthogonal in such a way that they form a complete basis, enabling us to express any $f(\mu)$ as in Eq. (61). The coefficients $f_l$ are the *Legendre multipoles*:

$$f_l = \frac{i^l}{2} \int_{-1}^{1} f(\mu) \mathcal{P}_l(\mu) \mathrm{d}\mu. \tag{62}$$

The factors $(2l + 1)/i^l$ in Eq. (61) and $i^l/2$ in Eq. (62) are just conventional choices. It is convenient to expand functions in this way when we are considering quantities that are function of a direction in the sky - since the Legendre polynomials are closely related to the spherical harmonics, which is a natural choice of basis for such quantities.

#### 4.1.3. Einstein-Boltzmann equations

We have two perturbations to the metric, $\Phi(\mathbf{x}, t)$ to the spatial curvature, and $\Psi(\mathbf{x}, t)$ to the Newtonian potential. We seek to find the effect of these perturbations on baryonic matter, dark energy and radiation, as they "live" in a now perturbed spacetime. Let's start by defining the perturbation to the photons, $\Theta(\mathbf{x}, \hat{\mathbf{p}}, t)$, to be the variation of photon temperature around an equilibrium temperature $T^{(0)}$:

$$T(\mathbf{x}, \hat{\mathbf{p}}, t) = T^{(0)} \left[1 + \Theta(\mathbf{x}, \hat{\mathbf{p}}, t)\right]. \tag{63}$$

This is dependent on the location $\mathbf{x}$ and the direction of propagation $\hat{\mathbf{p}}$, thus capturing both inhomogeneities and anisotropies. We assume $\Theta$ to be independent of the momentum magnitude.[16] The collision terms for the photons are governed by Compton scattering. We use the form found in (Dodelson & Schmidt 2020, Eq. 5.22)TODO: assumptions: ignore polarisation, and angular dep. of thomson cross sec:

$$C[f(\mathbf{p})] = -p^2 \frac{\partial f^{(0)}}{\partial p} n_e \sigma_T [\Theta_0 - \Theta(\hat{\mathbf{p}}) + \hat{\mathbf{p}} \cdot \mathbf{v}_b] \tag{64}$$

where $\Theta_0$ is the monopole term.[17] $\mathbf{v}_b$ is the bulk velocity of the electrons involved in the process, and is the same as for baryons, hence the subscript. The distribution function for radiation follows the Bose-Einstein distribution function, so we expand $f$ around its zeroth order Bose-Einstein form, (Dodelson & Schmidt 2020, Eq. 5.2-5.9), using the temperature perturbation in Eq. (63)TODO: Include equation 5.9 in Dodelson?. This is then inserted into Eq. (57), which we equate to the collision term in Eq. (64) in order to obtain the following full Boltzmann equation for radiation:[18]

$$\frac{\mathrm{d}\Theta}{\mathrm{d}t} + \frac{\hat{p}^i}{a} \frac{\partial \Theta}{\partial x^i} + \frac{\mathrm{d}\Phi}{\mathrm{d}t} + \frac{\hat{p}^i}{a} \frac{\partial \Psi}{\partial x^i} = n_e \sigma_T \left[\Theta_0 - \Theta + \hat{\mathbf{p}} \cdot \mathbf{v}_b\right] \tag{65}$$

For massive particles, we start with cold dark matter (CDM). Firstly, we assume cold dark matter to not interact with any other species, nor self-interact. Thus, we do not have any collision terms. Further, we also assume it to behave like a fluid, neglecting any terms not to first order. We consider cold dark matter to be non-relativistic, thus they will only have a sizeable monopole and dipole term, which means that the evolution is fully characterised by the density and velocity, Winther et al. (2023). TODO: how much about moments should I explain? Therefore, we take the first and second moment of Eq. (57) and consider them to first order, in order to retrieve the cosmological generalisation of the continuity equation (Dodelson & Schmidt 2020, Eq. 5.41):

$$\frac{\partial n_c}{\partial t} + \frac{1}{a} \frac{\partial (n_c v_c^i)}{\partial x^i} + 3\left[H + \frac{\partial \Phi}{\partial t}\right] n_c = 0, \tag{66}$$

and the Euler equation (Dodelson & Schmidt 2020, Eq. 5.50):

$$\frac{\partial v_c^i}{\partial t} + H v_c^i + \frac{1}{a} \frac{\partial \Psi}{\partial x^i} = 0. \tag{67}$$

In both Eq. (66) and Eq. (67), $n_c$ is the cold dark matter number density, $\mathbf{v}_c$ its bulk velocity. We then consider the perturbation of $n_c$ to first order:

$$n_c(\mathbf{x}, t) = n_c^{(0)} [1 + \delta_c(\mathbf{x}, t)], \tag{68}$$

and consider the first order perturbation to Eq. (66):

$$\frac{\partial \delta_c}{\partial t} + \frac{1}{a} \frac{\partial v_c^i}{\partial x^i} + 3 \frac{\partial \Phi}{\partial t} = 0. \tag{69}$$

Eq. (69) and Eq. (67) now described the evolution of the density perturbation $\delta_c$ and bulk velocity $\mathbf{v}_c$ of cold dark matter.

For baryons (protons and electrons) we also assume them to behave like a non-relativistic fluid, so taking moments is a similar task as for cold dark matter. The only difference is that

[16] This follows from the fact that the magnitude of the photon momentum is virtually unchanged by the dominant form of interaction, Compton scattering Dodelson & Schmidt (2020).

[17] This is the integral over the photon perturbation at any given point, over all photon directions. It is given by

$$\Theta_0(\mathbf{x}, t) \equiv \frac{1}{4\pi} \int \mathrm{d}\Omega' \Theta(\mathbf{x}, \hat{\mathbf{p}}', t)$$

where $\Omega'$ is the solid angle spanned by $\hat{\mathbf{p}}'$ Dodelson & Schmidt (2020).

[18] Where of course $m = 0 \iff E = p$.

baryons interact with each other through Coulomb scattering and Compton scattering. We may ignore Compton scattering between protons and photons due to the small cross-section, but electrons are coupled to both photons and protons. Since the first moment of the Boltzmann equation represents conservations of particle number, and none of the above interactions changes the total baryon particle number, the continuity equation is identical to Eq. (66), but for baryons. We also have a baryon perturbation similar to Eq. (68), which altogether results in the following density perturbation for baryons:

$$\frac{\partial \delta_b}{\partial t} + \frac{1}{a}\frac{\partial v_b^i}{\partial x^i} + 3\frac{\partial \Phi}{\partial t} = 0. \tag{70}$$

For the Euler equation, we now have to consider the collision terms, where momentum is conserved, but transferred between the baryons and photons. This collision term is found from considering the first moment of the photon distribution and find the momentum transfer due to Compton scattering. According to Winther et al. (2023) the momentum transfer in the baryon equation is $-n_e\sigma_T R^{-1}(v_\gamma^i - v_b^i)$, where $R$ is defined in Eq. (48). The Euler equation for baryons, similar to Eq. (67), but with the momentum transfer as source term now yield:

$$\frac{\partial v_b^i}{\partial t} + Hv_b^i + \frac{1}{a}\frac{\partial \Psi}{\partial x^i} = -n_e\sigma_T R^{-1}(v_\gamma^i - v_b^i) \tag{71}$$

We have now acquired differential equations for the temperature fluctuations, $\Theta$ in Eq. (65), and the overdensities[19], $\delta_c$, $\delta_b$, and bulk velocities $v_c^i$ and $v_b^i$, of cold dark matter and baryons respectively in Eq. (69), Eq. (70), Eq. (67) and Eq. (71). In order to make these differential equations easier to solve we make the transformation into Fourier space. We do this by introducing $\mu$ as the cosine of the angle between the Fourier wave vector $\mathbf{k}$ and the direction of the photon $\mathbf{p}/|\mathbf{p}|$. Additionally, velocities are generally longitudinal which enables us to write:

$$\mu \equiv \frac{\mathbf{k}\cdot\mathbf{p}}{kp}$$
$$\mathbf{v} = i\hat{\mathbf{k}}v \tag{72}$$

This enables us to summarise the differential equations as follows, now in Fourier space, and the time derivative is with respect to conformal time $\eta$:

$$\dot{\Theta} = -ik\mu(\Theta+\Psi) - \dot{\Phi} - \dot{\tau}\left[\Theta_0 - \Theta + i\mu v_b - \frac{\mathcal{P}_2\Theta_2}{2}\right], \tag{73a}$$
$$\dot{\delta}_c = -3\dot{\Phi} + kv_c, \tag{73b}$$
$$\dot{v}_c = -k\Psi - \mathcal{H}v_c, \tag{73c}$$
$$\dot{\delta}_b = -3\dot{\Phi} + kv_b, \tag{73d}$$
$$\dot{v}_b = -k\Psi + \dot{\tau}R^{-1}(v_b + 3\Theta_1) - \mathcal{H}v_b. \tag{73e}$$

In Eq. (73a) and Eq. (73e) we define $\dot{\tau}$ from Eq. (44). Additionally, in Eq. (73a) we have included the term $\mathcal{P}_2\Theta_2/2$ in order to account for the angular dependency of Compton scattering previously ignored. We have also used that the photon velocity is proportional to the dipole $\Theta_1 = -v_\gamma/3$.

Our next step is to once again consider the perturbation to the metric in order to find out how the potentials $\Psi$ and $\Phi$ change with time. In short, this is done by computing the perturbed Christoffel symbols using Eq. (54), finding the Ricci tensor and Ricci scalar, and construct the perturbed Einstein tensor. We also have to find the perturbed energy-momentum Tensor, and then solve the Einstein equation in Eq. (1). The result yields the time evolution of $\Phi$ and $\Psi$, where we have from (Dodelson & Schmidt 2020, Eq. 6.41):

$$k^2\Phi + 3\mathcal{H}(\dot{\Phi} - \mathcal{H}\Psi) = 4\pi Ga^2(\rho_c\delta_c + \rho_b\delta_b + 4\rho_\gamma\Theta_0), \tag{74}$$

and from (Dodelson & Schmidt 2020, Eq. 6.47)

$$k^2(\Phi+\Psi) = -32\pi Ga^2(\rho_\gamma\Theta_2): \tag{75}$$

Eq. (74) and Eq. (75) are both written in Fourier space. The final step is to write the photon fluctuations $\Theta$ as a hierarchy of multipoles in accordance with Eq. (61). The resultant hierarchy, along with all relevant equations, now written in terms of our preferred temporal variable $x$ is given below:

**Photon temperature multipoles**

$$\Theta_0' = -\frac{ck}{\mathcal{H}}\Theta_1 - \Phi', \tag{76a}$$
$$\Theta_1' = \frac{ck}{3\mathcal{H}}\Theta_0 - \frac{2ck}{3\mathcal{H}}\Theta_2 + \frac{ck}{3\mathcal{H}}\Psi + \tau'\left[\Theta_1 + \frac{1}{3}v_b\right], \tag{76b}$$
$$\Theta_l' = \begin{cases} \frac{lck\Theta_{l-1}}{(2l+1)\mathcal{H}} - \frac{(l+1)ck\Theta_{l+1}}{(2l+1)\mathcal{H}} + \tau'\left[\Theta_l - \frac{\Theta_2}{10}\delta_{l,2}\right], & l \geq 2 \\ \frac{ck\Theta_{l-1}}{\mathcal{H}} - c\frac{(l+1)\Theta_l}{\mathcal{H}\eta} + \tau'\Theta_l, & l = l_\mathrm{f} \end{cases} \tag{76c}$$

**Cold dark matter and baryons**

$$\delta_c' = \frac{ck}{\mathcal{H}}v_c - 3\Phi', \tag{77a}$$
$$v_c' = -v_c - \frac{ck}{\mathcal{H}}\Psi, \tag{77b}$$
$$\delta_b' = \frac{ck}{\mathcal{H}}v_b - 3\Phi', \tag{77c}$$
$$v_b' = -v_b - \frac{ck}{\mathcal{H}}\Psi + \tau' R^{-1}(3\Theta_1 + v_b) \tag{77d}$$

**Metric perturbations**

$$\Phi' = \Psi - \frac{c^2k^2}{3\mathcal{H}^2}\Phi + \frac{\mathcal{Y}}{2}, \tag{78a}$$
$$\Psi = -\Phi - \frac{12\mathcal{H}^2}{c^2k^2}\Omega_\gamma\Theta_2. \tag{78b}$$

where $\mathcal{Y} = \Omega_c\delta_c + \Omega_b\delta_b + 4\Omega_\gamma\Theta_0$

#### 4.1.4. Tight coupling regime

The tight coupling regime represents the time in the early Universe, before recombination, when both radiation, dark matter and baryons were tightly coupled together, interactions where frequent and efficient, and the primordial plasma very optically thick ($\tau \gg 1$). Due to this, the bulk velocity of the baryons (which co-moves with the other species due to the tight coupling) is very low. Furthermore, due to the frequent interactions and low bulk velocity the radiation dipole is suppressed. Altogether, this causes the combination $(3\Theta_1 + v_b)$ to be very small. The optical depth changes rapidly in the tight coupling regime, as seen from Fig. 12, $|\tau'| \gg 1$. As a result, any combinations of

[19] The fluctuations to the equilibrium densities.

the form $\tau'(\Theta_1 + v_b)$, as they occur in Eq. (76b) and Eq. (77d) are extremely numerically unstable. We therefore use said equations in order to rewrite for:

$$q = \frac{ck}{\mathcal{H}}(\Theta_0 - 2\Theta_2) + \tau'(1 + R^{-1})(3\Theta_1 + v_b) - v_b, \quad (79)$$

where we have defined

$$q \equiv (3\Theta_1 + v_b)' \implies \Theta_1' = (q - v_b')/3 \quad (80)$$

We are able to differentiate Eq. (79) w.r.t. $x$ by using $(R^{-1})' = -R^{-1}$ in order to obtain:

$$\begin{aligned} q' &= \left[\tau''\left(1+R^{-1}\right) + \left(1-R^{-1}\right)\tau'\right](3\Theta_1 + v_b) \\ &+ \left[\tau'\left(1+R^{-1}\right) - 1\right] q \\ &+ \frac{ck}{\mathcal{H}}\left(\Theta_0 - 2\Theta_2 + \Psi + \Theta_0' - 2\Theta_2' - \frac{\mathcal{H}'}{\mathcal{H}}(\Theta_0 - 2\Theta_2)\right) \end{aligned} \quad (81)$$

The treatment leading up to Eq. (81) is exact, but now we make the following approximation, Winther et al. (2023): In a radiation dominated universe (which is what we have in the tight coupling regime) we have that:

$$\begin{aligned} \eta \propto a \propto \tau'^{-1} \propto (3\Theta_1 + v_b) &\implies \frac{d^2}{d\eta^2}(3\Theta_1 + v_b) \approx 0 \\ &\implies q' \approx -\frac{\mathcal{H}'}{\mathcal{H}} q \end{aligned} \quad (82)$$

We find $q$ by equating Eq. (81) and Eq. (82) and solving for $q$. We further use Eq. (79) and solve for $\tau'(1 + R^{-1})(3\Theta_1 + v_b)$ which we substitute into Eq. (77d) in order to obtain an equation for $v_b'$. Altogether, this give rise to the following equations, valid in the tight coupling regime:

**Tight coupling equations**

$$\begin{aligned} q&\left[(1+R^{-1})\tau' + \frac{\mathcal{H}'}{\mathcal{H}} - 1\right] = \\ &-\left[\tau''\left(1+R^{-1}\right) + \left(1-R^{-1}\right)\tau'\right](3\Theta_1 + v_b) \\ &-\frac{ck}{\mathcal{H}}\Psi + \left(1 - \frac{\mathcal{H}'}{\mathcal{H}}\right)\frac{ck}{\mathcal{H}}(-\Theta_0 + 2\Theta_2) - \frac{ck}{\mathcal{H}}\Theta_0' \end{aligned} \quad (83)$$

$$\begin{aligned} v_b'\left[1 + R^{-1}\right] &= -v_b - \frac{ck}{\mathcal{H}}\Psi \\ &+ R^{-1}\left(q + \frac{ck}{\mathcal{H}}(-\Theta_0 + 2\Theta_2) - \frac{ck}{\mathcal{H}}\Psi\right) \end{aligned} \quad (84)$$

$$\Theta_1' = \frac{1}{3}(q - v_b'), \quad (85a)$$

$$\Theta_2 = -\frac{20ck}{45\mathcal{H}\tau'}\Theta_1, \quad (85b)$$

$$\Theta_l = -\frac{l}{2l+1}\frac{ck}{\mathcal{H}\tau'}\Theta_{l-1} \quad l > 2. \quad (85c)$$

#### 4.1.5. Inflation

To be able to numerically integrate Eq. (76), Eq. (77) and Eq. (78) we must determine the initial conditions of each quantity. Thus, we need to know how the Universe behaved at a very early stage. It is proposed that an epoch called *inflation* took place, during which the Universe exponentially increases in size during a very short period of time Dodelson & Schmidt (2020).[20] We will describe the inflationary period in order to obtain the initial conditions of the metric perturbations $\Psi$ and $\Phi$.

Assume inflation is driven by a scalar field $\psi(t, \mathbf{x})$, typically referred to as *inflaton field*. For inflation to happen, the acceleration of the scale factor must be positive, meaning that the inflaton field must model a fluid where the equation of state parameter $\omega$ is negative, i.e. $3p + \rho < 0$. By considering the temporal and spatial part of the energy-momentum tensor, Dodelson & Schmidt (2020) obtains the following equations for the pressure and density of the inflaton field:

$$\rho_\phi = \frac{1}{2}\left(\frac{d\phi}{dt}\right)^2 + V(\phi), \quad (86)$$

and

$$p_\phi = \frac{1}{2}\left(\frac{d\phi}{dt}\right)^2 - V(\phi), \quad (87)$$

where $1/2\left(\frac{d\phi}{dt}\right)^2$ is the kinetic energy of the field, and $V(\phi)$ is the potential energy. Thus, $\omega = p/\rho < 0$ implies that the inflaton field must have more potential than kinetic energy. We therefore require it to *roll slowly* in the potential, and thus introduce the *slow roll parameters* $\epsilon_{sr}$ and $\delta_{sr}$, both of which must be satisfied for the field to be able to perform inflation. These are:

$$\epsilon_{sr} = \frac{E_{pl}^2}{16\pi}\left(\frac{V'}{V}\right)^2 \ll 1 \quad (88a)$$

$$\delta_{sr} = \frac{E_{pl}}{8\pi}\left(\frac{V''}{V}\right) \ll 1, \quad (88b)$$

where the derivative of the potential $V$ is in terms of $\phi$.

Next, one of the crucial assumptions is that we can express the inflaton field in terms of a perturbation (or overdensity) as:

$$\phi(t, \mathbf{x}) = \phi^{(0)}(t) + \delta\phi(t, \mathbf{x}), \quad (89)$$

where $\phi^{(0)}$ is the equilibrium value of the field, only dependent on time. We will concern ourselves with the perturbation $\delta\phi$ and investigate what happens to it during the inflationary period. Before inflation, we expect $\Psi = \Phi = 0$ and the perturbation $\delta\phi$ to be of quantum nature.

TODO: fill more here maybe

We could in principle solve the full Einstein equation where $\Psi$ and $\Phi$ enters through the Einstein tensor, and $\phi$ through the energy-momentum tensor.[21] This is not trivial, and instead we

[20] An inflationary process would also solve the horizon problem, the flatness problem and the monopole problem amongst other things. Details about this can be found in both Dodelson & Schmidt (2020), Carroll (2019), and Weinberg (2008).

[21] The energy-momentum tensor for $\phi$ is given in (Dodelson & Schmidt 2020, Eq. 7.6) as:

$$T^\alpha{}_\beta = g^{\alpha\nu}\frac{\partial\phi}{\partial x^\nu}\frac{\partial\phi}{\partial x^\beta} - \delta^\alpha{}_\beta\left[\frac{1}{2}g^{\mu\nu}\frac{\partial\phi}{\partial x^\mu}\frac{\partial\phi}{\partial x^\nu} + V(\phi)\right].$$

introduce the curvature perturbation $\mathcal{R}(\delta\phi, \Psi)$, which is a conserved quantity, as Dodelson & Schmidt (2020):

$$\mathcal{R} = -\frac{ik_i \delta T_i^0}{k^2(p+\rho)} - \Psi, \tag{90}$$

where $k$ is the mode (in Fourier space), $T_0^i = g^{iv} = \partial_v\phi\partial_0\phi$ is the spatial part of the energy-momentum tensor, and $p$ and $\rho$ are the pressure and density.

If we consider the situation before inflation, assume $\Psi = 0$. From Eq. (88) we have that $\rho + p = \dot{\phi}^2/a^2$ using conformal time. Further, according to (Dodelson & Schmidt 2020, Eq. 7.47), $\delta T_0^i = ik_i\dot{\phi}\delta\phi/a^3$. Inserting this into Eq. (90) yield before inflation:

$$\mathcal{R}_{\text{initial}} = -aH\frac{\delta\phi}{\dot{\phi}}. \tag{91}$$

Looking at the same situation at the end of inflation, we now assume radiation domination: $p = \rho/3$. According to Dodelson & Schmidt (2020), $ik_i\delta T_0^i = -4k\rho_\gamma\Theta_1/a$ in the radiation dominated era. Inserting this into Eq. (90) yield:

$$\mathcal{R}_{\text{end}} = -\frac{3aH\Theta_1}{k} - \Psi = -\frac{3}{2}\Psi, \tag{92}$$

where the last equality comes from the postulate that the initial condition for the dipole is $\Theta_1 = -k\Phi/6aH$, which will we showed in the following section. For the sake of completeness, we not equate Eq. (91) and Eq. (92) to obtain:

$$\Psi = \frac{2}{3}aH\frac{\delta\phi}{\dot{\phi}}\Big|_{\text{horizon crossing}}, \tag{93}$$

which is the value of $\Psi$ immediately after inflation, when the mode is of equal size as the horizon (hence horizon crossing). TODO: check if this actually is correct

#### 4.1.6. Initial conditions

We now seek to determine the actual initial conditions enabling us to solve the desired differential equations. At very early times, we make the following assumptions:

$$k\eta \ll 1 \iff \frac{k}{\mathcal{H}} \ll 1 \tag{94a}$$
$$\tau \gg 1 \text{ and } |\tau'| \gg 1 \tag{94b}$$
$$\Theta_0 \gg \Theta_1 \gg \Theta_2 \gg \cdots \gg \Theta_l. \tag{94c}$$

Eq. (94a) is necessary in order to ensure causally disconnected regions in the early universe. It also ensures that the modes we are interested in today is outside the horizon Winther et al. (2023). We have already established that the universe is optically thick, so Eq. (94b) follow directly from Fig. 12. Further, at these scales we expect the lower multipoles to be dominant, thus Eq. (94c) holds. This is because the causal horizon is smaller than the $k$-modes, making the radiation observed by an hypothetical observer nearly uniform. Applying the assumptions in Eq. (94) to Eq. (76), Eq. (77) and Eq. (78) allows to determine the initial conditions.

Firstly, the perturbations of $\Phi$ and $\Psi$ evolves slowly outside the horizon, so we may approximate $\Phi' = \Psi' = 0$. However, we will use their expression in order to determine other initial conditions. In the following we make use of the assumptions in Eq. (94). Eq. (76a) becomes $\Theta_0' = -\Phi'$. Further, Eq. (78a) turn into $\Phi' = \Psi + 2\Theta_0 \implies \Theta_0 = -\Psi/2$. The overdensities Eq. (77c) and Eq. (77a) have similar behaviour[22] and we write $\delta' = -3\Phi' = 3\Theta_0'$. Integrating both sides yield $\delta = -3\Psi/2 + C$, where $C$ is the integration constant. This is put to zero, making the initial conditions *adiabatic*. Eq. (78b) now fixes the relation between the initial conditions of $\Psi$ and $\Phi$ as $\Phi = -\Psi$.

For the velocities, we expect the baryon and cold dark matter velocities to have the same initial value, and we find it by considering Eq. (77b), which can be written as $(va)' = -cka\Psi/\mathcal{H}$. Integration yields $v = -ck\Psi/2\mathcal{H}$ where we have omitted the constant of integration. We find the initial conditions for the next multipole terms by following a similar logic. This is also shown in (Dodelson & Schmidt 2020, Eq. 7.59) which fixes the velocities as $v = 3ck\Phi/6\mathcal{H}$,[23] and gives the initial dipole moment $\Theta_1 = -k\Phi/6aH$. Inserting this into Eq. (92) yields the desired $\mathcal{R} = -2\Psi/2$. Since $\mathcal{R}$ is conserved, choosing a value for it equations to fixing a normalisation. We will simply use $\mathcal{R} = 1$. The full set of adiabatic initial conditions then become:

**Initial conditions**

$$\Psi = -\frac{2}{3}, \tag{95a}$$
$$\Phi = -\Psi, \tag{95b}$$
$$\delta_c = \delta_b = -\frac{3}{2}\Psi, \tag{95c}$$
$$v_c = v_b = -\frac{ck}{2\mathcal{H}}\Psi, \tag{95d}$$
$$\Theta_0 = -\frac{1}{2}\Psi, \tag{95e}$$
$$\Theta_1 = \frac{ck}{6\mathcal{H}}\Psi, \tag{95f}$$
$$\Theta_2 = -\frac{20ck}{45\mathcal{H}\tau'}\Theta_1, \tag{95g}$$
$$\Theta_l = -\frac{l}{2l+1}\frac{ck}{\mathcal{H}\tau'}\Theta_{l-1}. \tag{95h}$$

### 4.2. Methods

some methods

### 4.3. Results and discussion

## References

Aghanim, N., Akrami, Y., Ashdown, M., et al. 2020, Astronomy & Astrophysics, 641, A6
Betoule, M., Kessler, R., Guy, J., et al. 2014, Astronomy & Astrophysics, 568, A22
Callin, P. 2006, How to calculate the CMB spectrum
Carroll, S. M. 2019, Spacetime and Geometry: An Introduction to General Relativity (Cambridge University Press)
Dodelson, S. & Schmidt, F. 2020, Modern Cosmology (Elsevier Science)
Ma, C.-P. & Bertschinger, E. 1995, The Astrophysical Journal, 455, 7
Weinberg, S. 2008, Cosmology, Cosmology (OUP Oxford)
Winther, H. A., Eriksen, H. K., Elgaroy, O., Mota, D. F., & Ihle, H. 2023, Cosmology II, https://cmb.wintherscoming.no/, accessed on March 1, 2023

[22] Because gravity does not care whether it acts on baryons or dark matter.

[23] Dodelson & Schmidt (2020) uses $iv$ as velocities, but we have multiplied the velocities with $i$ in order to make them real, but ultimately changing signs.

## Appendix A: Useful derivations

### A.1. Angular diameter distance

This is related to the physical distance of say, an object, whose extent is small compared to the distance at which we observe is. If the extension of the object is $\Delta s$, and we measure an angular size of $\Delta\theta$, then the angular distance to the object is:

$$d_A = \frac{\Delta s}{\Delta\theta} = \frac{\mathrm{d}s}{\mathrm{d}\theta} = \sqrt{e^{2x}r^2} = e^x r, \tag{A.1}$$

where we inserted for the line element $\mathrm{d}s$ as given in equation Eq. (2), and used the fact that $\mathrm{d}t/\mathrm{d}\theta = \mathrm{d}r/\mathrm{d}\theta = \mathrm{d}\phi/\mathrm{d}\theta = 0$ in polar coordinates.

### A.2. Luminosity distance

If the intrinsic luminosity, $L$ of an object is known, we can calculate the flux as: $F = L/(4\pi d_L^2)$, where $d_L$ is the luminosity distance. It is a measure of how much the light has dimmed when travelling from the source to the observer. For further analysis we observe that the luminosity of objects moving away from us is changing by a factor $a^{-4}$ due to the energy loss of electromagnetic radiation, and the observed flux is changed by a factor $1/(4\pi d_A^2)$. From this we draw the conclusion that the luminosity distance may be written as:

$$d_L = \sqrt{\frac{L}{4\pi F}} = \sqrt{\frac{d_A^2}{a^4}} = e^{-x}r \tag{A.2}$$

### A.3. Differential equations

From the definition of $e^x\mathrm{d}\eta = c\mathrm{d}t$ we have the following:

$$\begin{aligned} &\frac{\mathrm{d}\eta}{\mathrm{d}t} = \frac{\mathrm{d}\eta}{\mathrm{d}x}\frac{\mathrm{d}x}{\mathrm{d}t} = \frac{\mathrm{d}\eta}{\mathrm{d}x}H = e^{-x}c \\ \implies &\frac{\mathrm{d}\eta}{\mathrm{d}x} = \frac{c}{\mathcal{H}}. \end{aligned} \tag{A.3}$$

Likewise, for $t$ we have:

$$\begin{aligned} &\frac{\mathrm{d}\eta}{\mathrm{d}t} = \frac{\mathrm{d}\eta}{\mathrm{d}x}\frac{\mathrm{d}x}{\mathrm{d}t} = \frac{\mathrm{d}x}{\mathrm{d}t}\frac{c}{\mathcal{H}} = e^{-x}c \\ \implies &\frac{\mathrm{d}t}{\mathrm{d}x} = \frac{e^x}{\mathcal{H}} = \frac{1}{H}. \end{aligned} \tag{A.4}$$

## Appendix B: Sanity checks

### B.1. For $\mathcal{H}$

We start with the Hubble equation from Eq. (19) and realize that we may write any derivative of $U$ as

$$\frac{\mathrm{d}^n U}{\mathrm{d}x^n} = \sum_i(-\alpha_i)^n\Omega_{i0}e^{-\alpha_i x}. \tag{B.1}$$

We further have:

$$\frac{\mathrm{d}\mathcal{H}}{\mathrm{d}x} = \frac{H_0}{2}U^{-\frac{1}{2}}\frac{\mathrm{d}U}{\mathrm{d}x}, \tag{B.2}$$

and

$$\begin{aligned} \frac{\mathrm{d}^2\mathcal{H}}{\mathrm{d}x^2} &= \frac{\mathrm{d}}{\mathrm{d}x}\frac{\mathrm{d}\mathcal{H}}{\mathrm{d}x} \\ &= \frac{H_0}{2}\left[\frac{\mathrm{d}U}{\mathrm{d}x}\left(\frac{\mathrm{d}}{\mathrm{d}x}U^{-\frac{1}{2}}\right) + U^{-\frac{1}{2}}\left(\frac{\mathrm{d}}{\mathrm{d}x}\frac{\mathrm{d}U}{\mathrm{d}x}\right)\right] \\ &= H_0\left[\frac{1}{2U^{\frac{1}{2}}}\frac{\mathrm{d}^2U}{\mathrm{d}x^2} - \frac{1}{4U^{\frac{3}{2}}}\left(\frac{\mathrm{d}U}{\mathrm{d}x}\right)^2\right] \end{aligned} \tag{B.3}$$

Multiplying both equations with $\mathcal{H}^{-1} = 1/(H_0U^{\frac{1}{2}})$ yield the following:

$$\frac{1}{\mathcal{H}}\frac{\mathrm{d}\mathcal{H}}{\mathrm{d}x} = \frac{1}{2U}\frac{\mathrm{d}U}{\mathrm{d}x}, \tag{B.4}$$

and

$$\begin{aligned} \frac{1}{\mathcal{H}}\frac{\mathrm{d}^2\mathcal{H}}{\mathrm{d}x^2} &= \frac{1}{2U}\frac{\mathrm{d}^2U}{\mathrm{d}x^2} - \frac{1}{4U^2}\left(\frac{\mathrm{d}U}{\mathrm{d}x}\right)^2 \\ &= \frac{1}{2U}\frac{\mathrm{d}^2U}{\mathrm{d}x^2} - \left(\frac{1}{\mathcal{H}}\frac{\mathrm{d}U}{\mathrm{d}x}\right)^2 \end{aligned} \tag{B.5}$$

We now make the assumption that one of the density parameters dominate $\Omega_i >> \sum_{j\neq i}\Omega_i$, enabling the following approximation:

$$\begin{aligned} U &\approx \Omega_{i0}e^{-\alpha_i x} \\ \frac{\mathrm{d}^n U}{\mathrm{d}x^n} &\approx (-\alpha_i)^n\Omega_{i0}e^{-\alpha_i x}, \end{aligned} \tag{B.6}$$

from which we are able to construct:

$$\frac{1}{\mathcal{H}}\frac{\mathrm{d}\mathcal{H}}{\mathrm{d}x} \approx \frac{-\alpha_i\Omega_{i0}e^{-\alpha_i x}}{2\Omega_{i0}e^{-\alpha_i x}} = -\frac{\alpha_i}{2}, \tag{B.7}$$

and

$$\begin{aligned} \frac{1}{\mathcal{H}}\frac{\mathrm{d}^2\mathcal{H}}{\mathrm{d}x^2} &\approx \frac{\alpha_i^2\Omega_{i0}e^{-\alpha_i x}}{2\Omega_{i0}e^{-\alpha_i x}} - \left(\frac{\alpha_i}{2}\right)^2 \\ &= \frac{\alpha_i^2}{2} - \frac{\alpha_i^2}{4} = \frac{\alpha_i^2}{4} \end{aligned} \tag{B.8}$$

which are quantities which should be constant in different regimes and we can easily check if our implementation of $\mathcal{H}$ is correct, which is exactly what we sought.

### B.2. For $\eta$

TODO: fix this In order to test $\eta$ we consider the definition, solve the integral and consider the same regimes as above, where one density parameter dominates:

$$\begin{aligned} \eta &= \int_{-\infty}^{x}\frac{c\mathrm{d}x}{\mathcal{H}} = \frac{-2c}{\alpha_i}\int_{x=-\infty}^{x=x}\frac{\mathrm{d}\mathcal{H}}{\mathcal{H}^2} \\ &= \frac{2c}{\alpha_i}\left(\frac{1}{\mathcal{H}(x)} - \frac{1}{\mathcal{H}(-\infty)}\right), \end{aligned} \tag{B.9}$$

where we have used that:

$$\begin{aligned} &\frac{\mathrm{d}\mathcal{H}}{\mathrm{d}x} = -\frac{\alpha_i}{2}\mathcal{H} \\ \implies &\mathrm{d}x = -\frac{2}{\alpha_i\mathcal{H}}\mathrm{d}\mathcal{H}. \end{aligned} \tag{B.10}$$

Since we consider regimes where one density parameter dominates, we have that $\mathcal{H}(x) \propto \sqrt{e^{-\alpha_i x}}$, meaning that we have:

$$\left(\frac{1}{\mathcal{H}(x)} - \frac{1}{\mathcal{H}(-\infty)}\right) \approx \begin{cases} \frac{1}{\mathcal{H}} & \alpha_i > 0 \\ -\infty & \alpha_i < 0. \end{cases} \tag{B.11}$$

Combining the above yields:

$$\frac{\eta\mathcal{H}}{c} \approx \begin{cases} \frac{2}{\alpha_i} & \alpha_i > 0 \\ \infty & \alpha_i < 0. \end{cases} \tag{B.12}$$

Notice the positive sign before $\infty$. This is due to $\alpha_i$ now being negative.